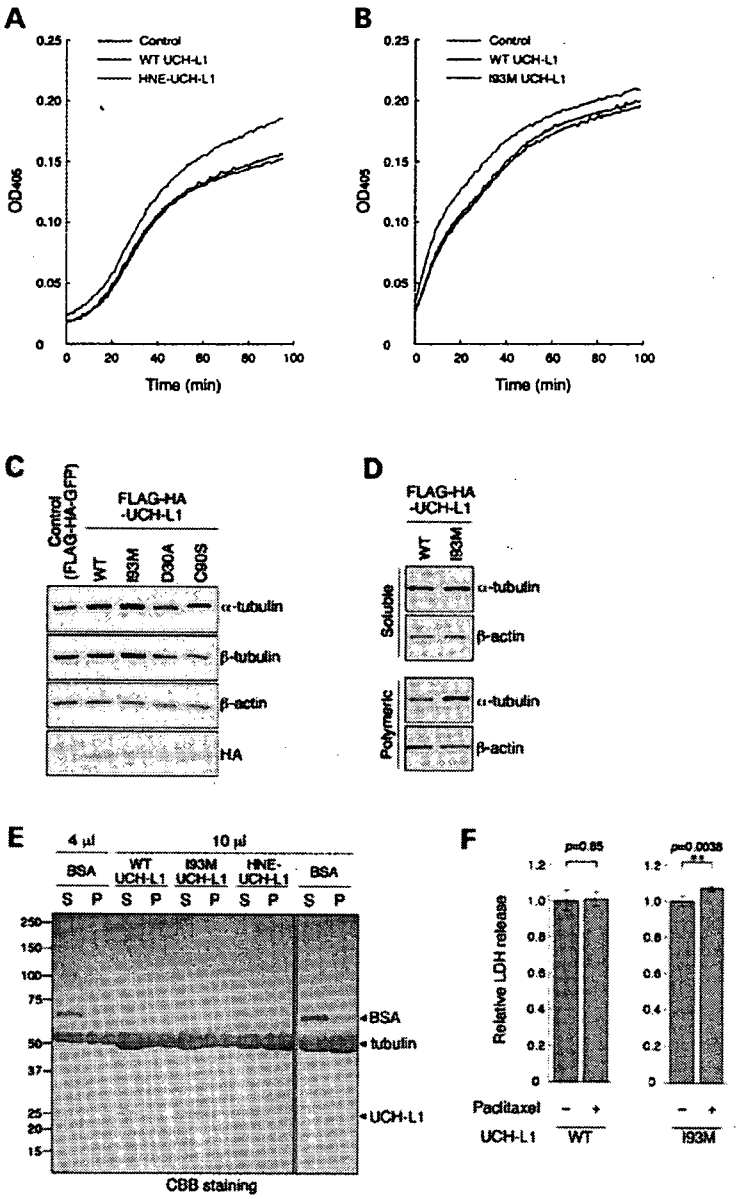

Figure 6. Effects of the I93M mutation and HNE modification of UCH-L1 on tubulin polymerization. [(**A**) and (**B**)] A tubulin polymerization assay was performed in the absence (control) or in the presence of recombinant UCH-L1. The assays were performed at least three times; representative results are shown. [(C) and (**D**)] Total lysates (C), soluble tubulin fractions and polymeric tubulin fractions (D) of NIH-3T3 cells stably expressing FLAG-HA-tagged UCH-L1 were analyzed by immunoblotting. (**E**) Interactions of proteins with microtubules. After the tubulin polymerization assay, the polymerized tubulin was pelleted by centrifugation. The indicated volumes of samples from the supernatants (S) and the pellets (P) were analyzed by CBB staining. BSA was used as a control that does not specifically interact with microtubules. The amount of BSA detected in the pellet fraction was approximately one-twelfth of the amount detected in the supernatant fraction. UCH-L1 levels in the pellet fraction were below detectable levels. (**F**) Differentiated Neuro2a cells transfected with the indicated constructs were incubated with or without 5 μM paclitaxel for 24 h. Cell death was assessed by a lactate dehydrogenase release assay. Data are expressed as the means ± SD ($n = 4$). $^{**}P < 0.01$ (*t*-test).

DISCUSSION

Our previous study using CD suggests that the I93M mutation increases the β-sheet content, but reduces the α-helix content of UCH-L1 (9). We have also shown, using small-angle neutron scattering, that UCH-L1^{WT} has an ellipsoidal shape, whereas UCH-L1^{I93M} has a more globular shape in an aqueous solution (10). However, the biochemical and molecular properties of UCH-L1^{I93M} in mammalian cells, as well as the molecular mechanisms that underlie UCH-L1^{I93M}-associated PD, have not been elucidated. In this study, we have shown that, compared with UCH-L1^{WT}, UCH-L1^{I93M} displays

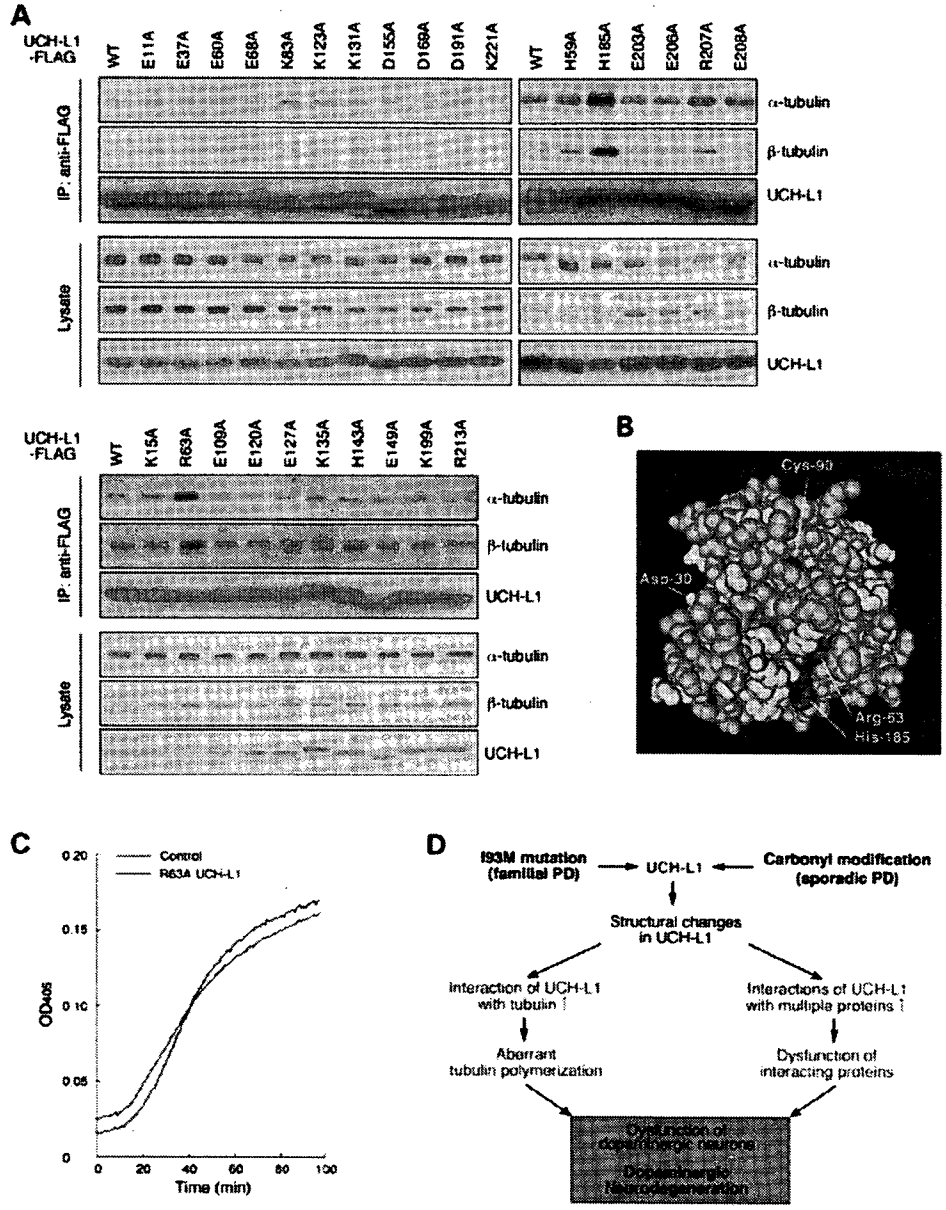

Figure 7. Amino acid residues of UCH-L1 involved in the interaction with tubulin. (**A**) Alanine-scanning mutagenesis of UCH-L1. Lysates of COS-7 cells transfected with the indicated constructs were immunoprecipitated with anti-FLAG antibody and analyzed by immunoblotting. (**B**) Structural model for human UCH-L1. Cys-90 is shown in blue, Arg-63 and His-185 are in magenta and basic and acidic amino acid residues that had no effect on tubulin interaction (Figs 5B and7A) are shown in white, using NCBI's structural model (mmdbId:38174). (**C**) A tubulin polymerization assay was performed in the absence (control) or in the presence of recombinant UCH-L1. (**D**) Schematic representation of a model for the roles of UCH-L1^{I93M} and carbonyl-modified UCH-L1 in PD. The I93M mutation (as occurs in familial PD associated with UCH-L1^{I93M}) and carbonyl modification (as occurs in sporadic PD) cause conformational changes in UCH-L1. Owing to the excess of oxidative stresses including HNE (in the case of sporadic PD) and the abundant expression of UCH-L1 in dopaminergic neurons, abnormal UCH-L1 proteins are overproduced in dopaminergic neurons. Abnormal UCH-L1 interacts with tubulin and aberrantly modulates tubulin polymerization. The aberrant interactions of UCH-L1 variants with multiple proteins may also cause dysfunctions of interacting proteins. The deregulations of abnormal UCH-L1-interacting proteins, including tubulin, result in dysfunction of dopaminergic neurons, leading to neurodegeneration.

increased insolubility, which is characteristic of several neurodegenerative disease-linked mutants, aberrantly elevated interactions with multiple proteins over 30 kDa and decreased interaction with monoubiquitin (Fig. 1). Taken together, our new and previous findings indicate that the I93M mutation in UCH-L1 alters its conformation, resulting in changes in the biochemical properties of UCH-L1.

Similar to UCH-L1^{I93M}, other dominantly inherited neurodegenerative disease-linked mutants, such as mutant SOD1 and mutant α-synuclein, cause neurodegeneration, presumably

via an acquired toxicity. Studies of the mutants strongly suggest that abnormally increased interactions of these mutant proteins with other proteins constitute a cause of disease (22–25). Therefore we screened for UCH-L1-interacting proteins using a coIP assay and subsequent LC-MS/MS analysis. We found that tubulin is a novel UCH-L1-interacting protein, and that the interactions of UCH-L1^{I93M} with these proteins are increased compared with those of UCH-L1^{WT} (Fig. 5B). We have also shown that UCH-L1^{I93M} promotes tubulin polymerization and stabilizes microtubules (Fig. 6B–D). UCH-L1^{I93M} and paclitaxel coordinately induced neuronal cell death (Fig. 6F). Together with the fact that tightly regulated tubulin polymerization is essential for neurons to function and remain viable, and that abnormal microtubule dynamics and tubulin polymerization are associated with several neurodegenerative diseases (37,38), our results strongly suggest that aberrant tubulin polymerization caused by mutant UCH-L1 at least partly constitutes a toxic function of mutant UCH-L1. Other than tubulin, mutant UCH-L1 interacts with multiple proteins (Figs 1F and 5A). These other interactors may also be involved in the mechanism of UCH-L1-mediated neurodegeneration (Fig. 7D). We have identified some of these interactors (T.K. and K.W., unpublished data), and these proteins are currently under investigation.

It is known that the majority of PD cases occur sporadically, and that oxidative/carbonyl stresses are elevated in PD brains (12,13). However, the molecular mechanisms underlying the causes of sporadic PD have remained largely unknown. Choi *et al.* (12) have shown that UCH-L1 is a major target of carbonyl damage associated with sporadic PD, implying that carbonyl-modified UCH-L1 is involved in the cause of these sporadic diseases. In the present study, we found that carbonyl-modified UCH-L1 and UCH-L1^{I93M} share molecular and functional properties. Importantly, both UCH-L1s display shared properties in all of the experiments we performed (Supplementary Material, Table S2). These results strongly suggest that carbonyl-modified UCH-L1 is also toxic to neurons and constitutes one of the causes of sporadic PD. Considering that UCH-L1 is abundant in the brain (5), and that UCH-L1 is a major target of carbonyl damage in PD brains (12), it is possible that carbonyl-modified UCH-L1 is the major cause of the disease.

It has been reported that UCH-L1 mRNA is expressed abundantly in dopaminergic neurons in the human brain (41). Abundant expression of UCH-L1 protein in dopaminergic neurons was also observed in mouse brains (Supplementary Material, Fig. S4 and S5). Dopaminergic neurons are particularly exposed to oxidative and carbonyl stresses because dopamine can auto-oxidize into toxic dopamine quinone, superoxide radicals and hydrogen peroxide (42). In addition, it has been reported that oxidative stresses in dopaminergic neurons in sporadic PD brains are higher than the stresses in control brains (30). Thus, in PD, UCH-L1^{I93M} or oxidative/carbonyl-modified UCH-L1 is possibly overproduced in dopaminergic neurons, leading to the selective loss of dopaminergic neurons (Fig. 7D).

Oxidatively modified UCH-L1 has also been found in the brains of both familial and sporadic Alzheimer's disease (AD) patients (12,43,44). AD is characterized pathologically by deposition of the amyloid β-protein in the form of amyloid plaques in the brain, and the deposition of the amyloid β is thought to be a major cause of both familial and sporadic AD (20). Thus, although it is possible that toxicity of carbonyl-modified UCH-L1 is involved in amyloid β-mediated neurodegeneration in AD, carbonyl-modified UCH-L1 may not be the primary cause of AD. A recent report has shown that brains from patients with sporadic PD and AD contain decreased levels of UCH-L1 (30 and 50% decrease, respectively) (12). Gong *et al.* (45) showed that the introduction of exogenous UCH-L1 rescued the synaptic and cognitive functions of AD model mice, which exhibit decreased levels of UCH-L1 in their hippocampi. We have also shown that mice deficient in UCH-L1 exhibit memory dysfunction (46). These findings indicate that a reduction in the levels of functional UCH-L1 may contribute to the pathogenesis of AD. Oxidative modification of several proteins, including antioxidant proteins, is found in mice deficient in UCH-L1 (47), suggesting involvement of these proteins in AD. Since diminution of the proteasome activity may lead to neurodegeneration (48), it is also possible that decreased UCH-L1 function leads to dysfunction of the ubiquitin-proteasome system and this dysfunction contributes to neurodegeneration in AD. On the contrary, mice deficient in UCH-L1 do not exhibit progressive dopaminergic cell loss, indicating that a loss or decrease in the level of UCH-L1 is not the main cause of PD. Investigation of the relationship between the specificity of brain areas that is affected by oxidative stress and genetic or environmental factors should generate further insights into the mechanism of oxidative stress in the pathogenesis of sporadic PD and AD.

In conclusion, familial PD-associated UCH-L1^{I93M} and carbonyl-modified UCH-L1, which is associated with sporadic PD, display common aberrant properties. Thus, UCH-L1^{I93M} is a useful tool for studying the molecular mechanism underlying sporadic PD. We propose that the abnormal interactions of UCH-L1 variants with other proteins including tubulin constitute one of the causes of not only familial PD associated with UCH-L1^{I93M}, but also sporadic PD, and can be therapeutic targets for these diseases and possibly for other neurodegenerative diseases.

MATERIALS AND METHODS

Plasmids

pCI-neo-hUCH-L1 plasmids containing human WT UCH-L1 and UCH-L1 variants with or without FLAG tag were prepared as described previously (49) or generated using a QuikChange Site-Directed Mutagenesis Kit (Stratagene, La Jolla, CA, USA). The expression plasmid pCR3-hα-synuclein containing FLAG-tagged human α-synuclein was kindly donated by Ryosuke Takahashi (Kyoto University, Kyoto, Japan) and Yuzuru Imai (Tohoku University, Miyagi, Japan) (50). The pcDNA3-hSOD1 expression plasmids containing WT, A4V, G85R or G93A mutant SOD1, and pCI-hα-synuclein expression plasmids containing WT, A30P or A53T mutant α-synuclein were prepared as described previously (17). The expression plasmid pEF-hUCH-L1 containing WT UCH-L1 was constructed by ligating the cDNA

encoding UCH-L1 into pEF-BOS vector (51). The bacterial expression plasmid pPROTetE-hUCH-L1 containing 6HN-tagged UCH-L1 was prepared as described previously. pGEX-hUCH-L1 bacterial expression plasmids containing WT, I93M or R63A UCH-L1 with a GST-tag were constructed by ligating the cDNA encoding each UCH-L1 into pGEX-6P-1 vector (GE Healthcare UK Ltd, Buckinghamshire HP7 9NA, UK).

Cell culture and transfection

Neuro2a, SH-SY5Y, COS-7 and HeLa cells were maintained in Dulbecco's modified Eagle's medium (Sigma, St Louis, MO, USA) supplemented with 10% fetal bovine serum (JRH Biosciences, Lenexa, KS, USA). NIH-3T3 cells stably expressing human UCH-L1 with a FLAG-HA double-tag at the N terminus were cultured as described previously (49). Transient transfection of Neuro2a, SH-SY5Y and COS-7 cells with each vector was performed using the FuGENE 6 Transfection Reagent (Roche Diagnostics, Indianapolis, IN, USA), TransFectin Lipid Reagent (Bio-Rad, Hercules, CA, USA) and Lipofectamine Reagent (Invitrogen, Carlsbad, CA, USA), respectively. For the experiments investigating the carbonyl modification of UCH-L1, cells were incubated at 37°C for 90 min with each carbonyl compound or H_2O_2 in PBS containing 5 mM glucose, 0.3 mM $CaCl_2$ and 0.62 mM $MgCl_2$.

Immunoblotting

SDS–PAGE was performed under reducing conditions. Immunoblotting was performed according to standard procedures. The preparation of detergent (1% Triton X-100)-soluble and -insoluble fractions was performed as described previously (17). Mouse anti-α-tubulin and anti-β-tubulin antibodies were purchased from Sigma. Rabbit anti-α-tubulin and anti-β-tubulin antibodies were from Cell Signaling (Danvers, MA, USA). Mouse anti-HNE and rabbit anti-HNE antibodies were from Oxis (Portland, OR, USA) and Alpha Diagnostic (San Antonio, TX, USA), respectively. Antibodies against SOD1, UCH-L1 and reduced-HNE were purchased from Stressgen Bioreagents (Victoria, BC, Canada), UltraClone (England, UK) and Calbiochem (Darmstadt, Germany), respectively. Anti-β-actin, ubiquitin and FLAG antibodies were from Sigma. The antibody against α-synuclein was from Chemicon (Temecula, CA, USA). For immunoblotting with anti-reduced HNE antibody, the proteins on a PVDF membrane were reduced with 10 mM $NaBH_4$ in Tris-buffered saline for 30 min at room temperature before being reacted with anti-reduced HNE antibody. Carbonyl modification of proteins was detected using an OxyBlot Protein Oxidation Detection Kit (Chemicon) containing an anti-DNP antibody.

Immunoprecipitation

Immunoprecipitation was performed as previously described (52). Cells were harvested by cold immunoprecipitation buffer (15 mM Tris pH 7.5, 120 mM NaCl, 25 mM KCl, 2 mM EGTA, 2 mM EDTA, 0.5% Triton X-100 and protease inhibitors). The lysates were centrifuged at 20 000*g* for 10 min at 4°C. The supernatant was subjected to immunoprecipitation. Lysates (1 mg protein in immunoprecipitation buffer) were incubated with 5 μg of antibody for 12 h. Twenty microliters of protein G Sepharose (GE Healthcare) was then added, and incubation was continued for 1 h. For the immunoprecipitation of FLAG-tagged proteins, lysates (1–2 mg protein in immunoprecipitation buffer) were incubated with 30 μl anti-FLAG M2 affinity gel (Sigma) for 2 h. After the beads were washed three times with immunoprecipitation buffer, proteins were eluted with SDS sample buffer (10 mM Tris, pH 7.8, 3% SDS, 5% glycerol and 0.02% bromophenol blue). In some experiments, proteins were eluted with SDS sample buffer containing 2% 2-mercaptoethanol. For the immunoprecipitation of endogenous UCH-L1 (Fig. 5D), 100 μg anti-UCH-L1 antibody (53) or 100 μg normal rabbit IgG (Santa Cruz Biotechnology, Santa Cruz, CA, USA) was immobilized to 100 μl of protein G beads using a Seize X Protein G Immnoprecipitation Kit (Pierce, Rockford, IL, USA). Cell lysates (1 mg protein in 50 mM Tris, pH 7.5, 150 mM NaCl, 5 mM EDTA, 0.25% Triton X-100 and protease inhibitors) were incubated with 25 μl of beads for 12 h. Protein G beads without antibody and protein G beads cross-linked with normal rabbit IgG were used as controls.

Mass spectrometry analysis

Protein bands were sliced from the gel and subjected to in-gel trypsin digestion, and LC-MS/MS analysis was performed at APRO Life Science Institute, Inc. (Naruto, Japan) as a custom service.

Circular dichroism

CD measurements of 0.1 mg/ml (4 μM) of recombinant human UCH-L1 without a tag (Boston Biochem, Cambridge, MA, USA) in 20 mM sodium phosphate buffer (pH 8.0) were performed as described previously (9,10). Since two cysteine residues in UCH-L1, Cys-90 and Cys-152, are major targets of HNE modification (Fig. 4), 4 μM UCH-L1 was reacted with 8 μM HNE. Far UV CD spectra (190–250 nm) were recorded in a 1 mm quartz cuvette on a Jasco J-820 spectropolarimeter (Jasco, Tokyo, Japan) equipped with a temperature controller by scanning at a rate of 50 nm/min at 25°C. For all spectra, 12 scans were averaged. All CD spectra were corrected by background subtraction of the spectrum obtained with buffer alone and smoothed. Spectra were analyzed for the percentage of secondary structural elements by a computer program, based on an algorithm that compares experimental spectra with those of known proteins (54).

Preparation of recombinant proteins

6HN-tagged human UCH-L1 proteins were prepared as described previously (9). For purification of UCH-L1 without a tag, the pGEX UCH-L1 vectors were transformed into *Escherichia coli* BL21. Production of fusion proteins was induced by the addition of isopropyl-β-D-thiogalactopyranoside to a final concentration of 0.5 mM. After a 4 h induction at 37°C, the cells were harvested and lysed by sonication in PBS containing 1% Triton X-100 and protease inhibitors. Puri-

fication of GST-tagged UCH-L1 was performed using glutathione Sepharose 4B (GE Healthcare), and UCH-L1 was released from GST by digestion using PreScission Protease (GE Healthcare). Purified proteins were resolved by SDS–PAGE under reducing conditions and visualized by Coomassie brilliant blue R-250 to confirm purity (Supplementary Material, Fig. S6).

Pull-down assay

TALON resin (Clontech, Palo Alto, CA, USA) was blocked with 3% BSA for 1 h in order to prevent non-specific binding of tubulin (data not shown) and washed three times with PBS containing 0.05% Triton X-100. Five micrograms of recombinant UCH-L1 with an HN tag and 5 μg of purified tubulin (>99% pure tubulin, Cytoskeleton, Denver, CO, USA) were mixed and incubated for 4 h in PBS containing 0.05% Triton X-100. As a control, vehicle was mixed instead of UCH-L1. Twenty microliters of TALON resin blocked with BSA was then added, and incubation was continued for 1 h. After beads were washed three times with PBS containing 0.05% Triton X-100, proteins were eluted with SDS sample buffer.

Tubulin polymerization assay

An *in vitro* tubulin polymerization assay was performed using a tubulin polymerization assay kit, OD based, >99% pure tubulin (Cytoskeleton), according to the manufacturer's protocol. Briefly, recombinant UCH-L1 without a tag and tubulin were mixed to give a final concentration of 0.05 mg/ml UCH-L1 and 3 mg/ml tubulin in tubulin polymerization buffer (80 mM PIPES, pH 6.9, 2 mM $MgCl_2$, 0.5 mM EGTA, 1 mM GTP, 5% glycerol) and subjected to a tubulin polymerization assay. As a control, vehicle was mixed instead of UCH-L1. Since two cysteine residues in UCH-L1 are major targets of HNE modification (Fig. 4), 40 μM UCH-L1 was reacted with 80 μM HNE to prepare the HNE-modified UCH-L1. To analyze the interaction between UCH-L1 and polymerized tubulin, the polymerized tubulin was pelleted by centrifugation after a tubulin polymerization assay. The supernatant (100 μl) was mixed with 50 μl of 3× SDS sample buffer (30 mM Tris, pH 7.8, 9% SDS, 15% glycerol, 0.06% bromophenol blue). The pellet was washed twice with tubulin polymerization buffer and then dissolved in 150 μl of SDS sample buffer.

Preparation of cell extracts containing soluble and polymeric tubulin

Preparation of soluble and polymeric fractions of tubulin was performed as described (55) with slight modification. Briefly, cells were washed very gently with a microtubule stabilizing buffer (0.1 M *N*-morpholinoethanesulfonic acid, pH 6.75, 1 mM $MgSO_4$, 2 mM EGTA, 0.1 mM EDTA, 4 M glycerol). Soluble proteins were extracted at 37°C for 5 min in microtubule stabilizing buffer containing 0.04% saponin. The remaining cytoskeletal fraction in the culture dish was washed with microtubule stabilizing buffer containing 0.4% saponin and dissolved in SDS sample buffer.

Quantitative assessment of cell death

Neuro2a cells were transfected with plasmids. Four hours after transfection, neuronal cell differentiation was induced by addition of 5 mM dibutyryl cAMP as described in the literature (40), and cells were incubated for 24 h. Cells were then incubated with or without 5 μM paclitaxel for another 24 h. Cell death was assessed by a lactate dehydrogenase release assay, as described previously (17).

Statistical analysis

For comparison of two groups, the statistical difference was determined by Student's *t*-test.

SUPPLEMENTARY MATERIAL

Supplementary Material is available at HMG Online.

ACKNOWLEDGEMENTS

We thank Dr Ryosuke Takahashi (Kyoto University) and Dr Yuzuru Imai (Tohoku University) for the gift of pCR3-hα-synuclein plasmid, Dr Yasuyuki Suzuki (National Institute of Neuroscience) for valuable discussion; Naoki Takagaki (National Institute of Neuroscience) for support with English.

Conflict of Interest statement. None declared.

FUNDING

This work was supported by Grants-in-Aid for Scientific Research of Japan Society for the Promotion of Science; Research Grant in Priority Area Research of the Ministry of Education, Culture, Sports, Science and Technology, Japan; Grants-in-Aid for Scientific Research of the Ministry of Health, Labour and Welfare, Japan; Program for Promotion of Fundamental Studies in Health Sciences of the National Institute of Biomedical Innovation (NIBIO), Japan; New Energy and Industrial Technology Development Organization (NEDO), Japan.

REFERENCES

1. Leroy, E., Boyer, R., Auburger, G., Leube, B., Ulm, G., Mezey, E., Harta, G., Brownstein, M.J., Jonnalagada, S., Chernova, T. *et al.* (1998) The ubiquitin pathway in Parkinson's disease. *Nature*, **395**, 451–452.
2. Setsuie, R., Wang, Y.L., Mochizuki, H., Osaka, H., Hayakawa, H., Ichihara, N., Li, H., Furuta, A., Sano, Y., Sun, Y.J. *et al.* (2007) Dopaminergic neuronal loss in transgenic mice expressing the Parkinson's disease-associated UCH-L1 I93M mutant. *Neurochem. Int.*, **50**, 119–129.
3. Maraganore, D.M., Lesnick, T.G., Elbaz, A., Chartier-Harlin, M.C., Gasser, T., Kruger, R., Hattori, N., Mellick, G.D., Quattrone, A., Satoh, J. *et al.* (2004) UCHL1 is a Parkinson's disease susceptibility gene. *Ann. Neurol.*, **55**, 512–521.
4. Healy, D.G., Abou-Sleiman, P.M., Casas, J.P., Ahmadi, K.R., Lynch, T., Gandhi, S., Muqit, M.M., Foltynie, T., Barker, R., Bhatia, K.P. *et al.* (2006) UCHL-1 is not a Parkinson's disease susceptibility gene. *Ann. Neurol.*, **59**, 627–633.
5. Wilkinson, K.D., Lee, K.M., Deshpande, S., Duerksen-Hughes, P., Boss, J.M. and Pohl, J. (1989) The neuron-specific protein PGP 9.5 is a ubiquitin carboxyl-terminal hydrolase. *Science*, **246**, 670–673.

6. Larsen, C.N., Krantz, B.A. and Wilkinson, K.D. (1998) Substrate specificity of deubiquitinating enzymes: ubiquitin C-terminal hydrolases. *Biochemistry*, **37**, 3358–3368.
7. Liu, Y., Fallon, L., Lashuel, H.A., Liu, Z. and Lansbury, P.T., Jr (2002) The UCH-L1 gene encodes two opposing enzymatic activities that affect alpha-synuclein degradation and Parkinson's disease susceptibility. *Cell*, **111**, 209–218.
8. Osaka, H., Wang, Y.L., Takada, K., Takizawa, S., Setsuie, R., Li, H., Sato, Y., Nishikawa, K., Sun, Y.J., Sakurai, M. *et al.* (2003) Ubiquitin carboxy-terminal hydrolase L1 binds to and stabilizes monoubiquitin in neuron. *Hum. Mol. Genet.*, **12**, 1945–1958.
9. Nishikawa, K., Li, H., Kawamura, R., Osaka, H., Wang, Y.L., Hara, Y., Hirokawa, T., Manago, Y., Amano, T., Noda, M. *et al.* (2003) Alterations of structure and hydrolase activity of parkinsonism-associated human ubiquitin carboxyl-terminal hydrolase L1 variants. *Biochem. Biophys. Res. Commun.*, **304**, 176–183.
10. Naito, S., Mochizuki, H., Yasuda, T., Mizuno, Y., Furusaka, M., Ikeda, S., Adachi, T., Shimizu, H.M., Suzuki, J., Fujiwara, S. *et al.* (2006) Characterization of multimetric variants of ubiquitin carboxyl-terminal hydrolase L1 in water by small-angle neutron scattering. *Biochem. Biophys. Res. Commun.*, **339**, 717–725.
11. Saigoh, K., Wang, Y.L., Suh, J.G., Yamanishi, T., Sakai, Y., Kiyosawa, H., Harada, T., Ichihara, N., Wakana, S., Kikuchi, T. *et al.* (1999) Intragenic deletion in the gene encoding ubiquitin carboxy-terminal hydrolase in gad mice. *Nat. Genet.*, **23**, 47–51.
12. Choi, J., Levey, A.I., Weintraub, S.T., Rees, H.D., Gearing, M., Chin, L.S. and Li, L. (2004) Oxidative modifications and down-regulation of ubiquitin carboxyl-terminal hydrolase L1 associated with idiopathic Parkinson's and Alzheimer's diseases. *J. Biol. Chem.*, **279**, 13256–13264.
13. Ischiropoulos, H. and Beckman, J.S. (2003) Oxidative stress and nitration in neurodegeneration: cause, effect, or association? *J. Clin. Invest.*, **111**, 163–169.
14. Lowe, J., McDermott, H., Landon, M., Mayer, R.J. and Wilkinson, K.D. (1990) Ubiquitin carboxyl-terminal hydrolase (PGP 9.5) is selectively present in ubiquitinated inclusion bodies characteristic of human neurodegenerative diseases. *J. Pathol.*, **161**, 153–160.
15. Lee, M.K., Stirling, W., Xu, Y., Xu, X., Qui, D., Mandir, A.S., Dawson, T.M., Copeland, N.G., Jenkins, N.A. and Price, D.L. (2002) Human alpha-synuclein-harboring familial Parkinson's disease-linked Ala-53→Thr mutation causes neurodegenerative disease with alpha-synuclein aggregation in transgenic mice. *Proc. Natl Acad. Sci. USA*, **99**, 8968–8973.
16. Johnston, J.A., Dalton, M.J., Gurney, M.E. and Kopito, R.R. (2000) Formation of high molecular weight complexes of mutant Cu,Zn-superoxide dismutase in a mouse model for familial amyotrophic lateral sclerosis. *Proc. Natl Acad. Sci. USA*, **97**, 12571–12576.
17. Kabuta, T., Suzuki, Y. and Wada, K. (2006) Degradation of amyotrophic lateral sclerosis-linked mutant Cu,Zn-superoxide dismutase proteins by macroautophagy and the proteasome. *J. Biol. Chem.*, **281**, 30524–30533.
18. Lewis, J., McGowan, E., Rockwood, J., Melrose, H., Nacharaju, P., Van Slegtenhorst, M., Gwinn-Hardy, K., Paul Murphy, M., Baker, M., Yu, X. *et al.* (2000) Neurofibrillary tangles, amyotrophy and progressive motor disturbance in mice expressing mutant (P301L) tau protein. *Nat. Genet.*, **25**, 402–405.
19. Ardley, H.C., Scott, G.B., Rose, S.A., Tan, N.G. and Robinson, P.A. (2004) UCH-L1 aggresome formation in response to proteasome impairment indicates a role in inclusion formation in Parkinson's disease. *J. Neurochem.*, **90**, 379–391.
20. Haass, C. and Selkoe, D.J. (2007) Soluble protein oligomers in neurodegeneration: lessons from the Alzheimer's amyloid beta-peptide. *Nat. Rev. Mol. Cell Biol.*, **8**, 101–112.
21. Arrasate, M., Mitra, S., Schweitzer, E.S., Segal, M.R. and Finkbeiner, S. (2004) Inclusion body formation reduces levels of mutant huntingtin and the risk of neuronal death. *Nature*, **431**, 805–810.
22. Pasinelli, P., Belford, M.E., Lennon, N., Bacskai, B.J., Hyman, B.T., Trotti, D. and Brown, R.H., Jr (2004) Amyotrophic lateral sclerosis-associated SOD1 mutant proteins bind and aggregate with Bcl-2 in spinal cord mitochondria. *Neuron*, **43**, 19–30.
23. Zhang, F., Strom, A.L., Fukada, K., Lee, S., Hayward, L.J. and Zhu, H. (2007) Interaction between familial amyotrophic lateral sclerosis (ALS)-linked SOD1 mutants and the dynein complex. *J. Biol. Chem.*, **282**, 16691–16699.
24. Urushitani, M., Sik, A., Sakurai, T., Nukina, N., Takahashi, R. and Julien, J.P. (2006) Chromogranin-mediated secretion of mutant superoxide dismutase proteins linked to amyotrophic lateral sclerosis. *Nat. Neurosci.*, **9**, 108–118.
25. Cuervo, A.M., Stefanis, L., Fredenburg, R., Lansbury, P.T. and Sulzer, D. (2004) Impaired degradation of mutant alpha-synuclein by chaperone-mediated autophagy. *Science*, **305**, 1292–1295.
26. Schaffar, G., Breuer, P., Boteva, R., Behrends, C., Tzvetkov, N., Strippel, N., Sakahira, H., Siegers, K., Hayer-Hartl, M. and Hartl, F.U. (2004) Cellular toxicity of polyglutamine expansion proteins: mechanism of transcription factor deactivation. *Mol. Cell*, **15**, 95–105.
27. Uchida, K. (2000) Role of reactive aldehyde in cardiovascular diseases. *Free Radic. Biol. Med.*, **28**, 1685–1696.
28. Uchida, K. (2003) Histidine and lysine as targets of oxidative modification. *Amino Acids*, **25**, 249–257.
29. Stadtman, E.R. (1993) Oxidation of free amino acids and amino acid residues in proteins by radiolysis and by metal-catalyzed reactions. *Annu. Rev. Biochem.*, **62**, 797–821.
30. Yoritaka, A., Hattori, N., Uchida, K., Tanaka, M., Stadtman, E.R. and Mizuno, Y. (1996) Immunohistochemical detection of 4-hydroxynonenal protein adducts in Parkinson disease. *Proc. Natl Acad. Sci. USA*, **93**, 2696–2701.
31. Castellani, R.J., Perry, G., Siedlak, S.L., Nunomura, A., Shimohama, S., Zhang, J., Montine, T., Sayre, L.M. and Smith, M.A. (2002) Hydroxynonenal adducts indicate a role for lipid peroxidation in neocortical and brainstem Lewy bodies in humans. *Neurosci. Lett.*, **319**, 25–28.
32. Das, C., Hoang, Q.Q., Kreinbring, C.A., Luchansky, S.J., Meray, R.K., Ray, S.S., Lansbury, P.T., Ringe, D. and Petsko, G.A. (2006) Structural basis for conformational plasticity of the Parkinson's disease-associated ubiquitin hydrolase UCH-L1. *Proc. Natl Acad. Sci. USA*, **103**, 4675–4680.
33. Tiwari, A., Xu, Z. and Hayward, L.J. (2005) Aberrantly increased hydrophobicity shared by mutants of Cu,Zn-superoxide dismutase in familial amyotrophic lateral sclerosis. *J. Biol. Chem.*, **280**, 29771–29779.
34. Richardson, J.S. and Richardson, D.C. (2002) Natural beta-sheet proteins use negative design to avoid edge-to-edge aggregation. *Proc. Natl Acad. Sci. USA*, **99**, 2754–2759.
35. Lee, J.J. and Swain, S.M. (2006) Peripheral neuropathy induced by microtubule-stabilizing agents. *J. Clin. Oncol.*, **24**, 1633–1642.
36. Figueroa-Masot, X.A., Hetman, M., Higgins, M.J., Kokot, N. and Xia, Z. (2001) Taxol induces apoptosis in cortical neurons by a mechanism independent of Bcl-2 phosphorylation. *J. Neurosci.*, **21**, 4657–4667.
37. Panda, D., Samuel, J.C., Massie, M., Feinstein, S.C. and Wilson, L. (2003) Differential regulation of microtubule dynamics by three- and four-repeat tau: implications for the onset of neurodegenerative disease. *Proc. Natl Acad. Sci. USA*, **100**, 9548–9553.
38. Fanara, P., Banerjee, J., Hueck, R.V., Harper, M.R., Awada, M., Turner, H., Husted, K.H., Brandt, R. and Hellerstein, M.K. (2007) Stabilization of hyperdynamic microtubules is neuroprotective in amyotrophic lateral sclerosis. *J. Biol. Chem.*, **282**, 23465–23472.
39. Tam, S., Geller, R., Spiess, C. and Frydman, J. (2006) The chaperonin TRiC controls polyglutamine aggregation and toxicity through subunit-specific interactions. *Nat. Cell Biol.*, **8**, 1155–1162.
40. Kitamura, A., Kubota, H., Pack, C.G., Matsumoto, G., Hirayama, S., Takahashi, Y., Kimura, H., Kinjo, M., Morimoto, R.I. and Nagata, K. (2006) Cytosolic chaperonin prevents polyglutamine toxicity with altering the aggregation state. *Nat. Cell Biol.*, **8**, 1163–1170.
41. Solano, S.M., Miller, D.W., Augood, S.J., Young, A.B. and Penney, J.B., Jr (2000) Expression of alpha-synuclein, parkin, and ubiquitin carboxy-terminal hydrolase L1 mRNA in human brain: genes associated with familial Parkinson's disease. *Ann. Neurol.*, **47**, 201–210.
42. Lotharius, J. and Brundin, P. (2002) Pathogenesis of Parkinson's disease: dopamine, vesicles and alpha-synuclein. *Nat. Rev. Neurosci.*, **3**, 932–942.
43. Castegna, A., Aksenov, M., Aksenova, M., Thongboonkerd, V., Klein, J.B., Pierce, W.M., Booze, R., Markesbery, W.R. and Butterfield, D.A. (2002) Proteomic identification of oxidatively modified proteins in Alzheimer's disease brain. Part I: creatine kinase BB, glutamine synthase, and ubiquitin carboxy-terminal hydrolase L-1. *Free Radic. Biol. Med.*, **33**, 562–571.
44. Butterfield, D.A., Gnjec, A., Poon, H.F., Castegna, A., Pierce, W.M., Klein, J.B. and Martins, R.N. (2006) Redox proteomics identification of

oxidatively modified brain proteins in inherited Alzheimer's disease: an initial assessment. *J. Alzheimers Dis.*, **10**, 391–397.
45. Gong, B., Cao, Z., Zheng, P., Vitolo, O.V., Liu, S., Staniszewski, A., Moolman, D., Zhang, H., Shelanski, M. and Arancio, O. (2006) Ubiquitin hydrolase Uch-L1 rescues beta-amyloid-induced decreases in synaptic function and contextual memory. *Cell*, **126**, 775–788.
46. Sakurai, M., Sekiguchi, M., Zushida, K., Yamada, K., Nagamine, S., Kabuta, T. and Wada, K. (2008) Reduction of memory in passive avoidance learning, exploratory behavior and synaptic plasticity in mice with a spontaneous deletion in the ubiquitin C-terminal hydrolase L1 gene. *Eur. J. Neurosci.*, in press.
47. Castegna, A., Thongboonkerd, V., Klein, J., Lynn, B.C., Wang, Y.L., Osaka, H., Wada, K. and Butterfield, D.A. (2004) Proteomic analysis of brain proteins in the gracile axonal dystrophy (gad) mouse, a syndrome that emanates from dysfunctional ubiquitin carboxyl-terminal hydrolase L-1, reveals oxidation of key proteins. *J. Neurochem.*, **88**, 1540–1546.
48. Halliwell, B. (2006) Proteasomal dysfunction: a common feature of neurodegenerative diseases? Implications for the environmental origins of neurodegeneration. *Antioxid. Redox Signal.*, **8**, 2007–2019.
49. Sakurai, M., Ayukawa, K., Setsuie, R., Nishikawa, K., Hara, Y., Ohashi, H., Nishimoto, M., Abe, T., Kudo, Y., Sekiguchi, M. *et al.* (2006) Ubiquitin C-terminal hydrolase L1 regulates the morphology of neural progenitor cells and modulates their differentiation. *J. Cell Sci.*, **119**, 162–171.
50. Imai, Y., Soda, M. and Takahashi, R. (2000) Parkin suppresses unfolded protein stress-induced cell death through its E3 ubiquitin-protein ligase activity. *J. Biol. Chem.*, **275**, 35661–35664.
51. Mizushima, S. and Nagata, S. (1990) pEF-BOS, a powerful mammalian expression vector. *Nucleic Acids Res.*, **18**, 5322.
52. Kabuta, T., Hakuno, F., Asano, T. and Takahashi, S. (2002) Insulin receptor substrate-3 functions as transcriptional activator in the nucleus. *J. Biol. Chem.*, **277**, 6846–6851.
53. Sano, Y., Furuta, A., Setsuie, R., Kikuchi, H., Wang, Y.L., Sakurai, M., Kwon, J., Noda, M. and Wada, K. (2006) Photoreceptor cell apoptosis in the retinal degeneration of Uchl3-deficient mice. *Am. J. Pathol.*, **169**, 132–141.
54. Yang, J.T., Wu, C.S. and Martinez, H.M. (1986) Calculation of protein conformation from circular dichroism. *Methods Enzymol.*, **130**, 208–269.
55. Joshi, H.C. and Cleveland, D.W. (1989) Differential utilization of beta-tubulin isotypes in differentiating neurites. *J. Cell Biol.*, **109**, 663–673.

Available online at www.sciencedirect.com
ScienceDirect
Bioorganic & Medicinal Chemistry
ELSEVIER
Bioorganic & Medicinal Chemistry 15 (2007) 6810–6818

Identification of novel chemical inhibitors for ubiquitin C-terminal hydrolase-L3 by virtual screening

Kazunori Hirayama,[a,b] Shunsuke Aoki,[b,*] Kaori Nishikawa,[b] Takashi Matsumoto[a] and Keiji Wada[b]

[a]*Department of Electrical Engineering and Bioscience, Graduate School of Advanced Science and Engineering, Waseda University, 3-4-1 Okubo, Shinjuku-ku, Tokyo 169-8555, Japan*
[b]*Department of Degenerative Neurological Diseases, National Institute of Neuroscience, National Center of Neurology and Psychiatry, 4-1-1 Ogawa-Higashi, Kodaira, Tokyo 187-8502, Japan*

Received 11 May 2007; revised 14 July 2007; accepted 18 July 2007
Available online 19 August 2007

Abstract—UCH-L3 (ubiquitin C-terminal hydrolase-L3) is a de-ubiquitinating enzyme that is a component of the ubiquitin–proteasome system and known to be involved in programmed cell death. A previous study of high-throughput drug screening identified an isatin derivative as a UCH-L3 inhibitor. In this study, we attempted to identify a novel inhibitor with a different structural basis. We performed in silico structure-based drug design (SBDD) using human UCH-L3 crystal structure data (PDB code; 1XD3) and the virtual compound library (ChemBridge CNS-Set), which includes 32,799 chemicals. By a two-step virtual screening method using DOCK software (first screening) and GOLD software (second screening), we identified 10 compounds with GOLD scores of over 60. To address whether these compounds exhibit an inhibitory effect on the de-ubiquitinating activity of UCH-L3, we performed an enzymatic assay using ubiquitin-7-amido-4-methylcoumarin (Ub-AMC) as the substrate. As a result, we identified three compounds with similar basic dihydro-pyrrole skeletons as UCH-L3 inhibitors. These novel compounds may be useful for the research of UCH-L3 function, and in drug development for UCH-L3-associated diseases.

1. Introduction

The ubiquitin–proteasome system is responsible for the regulation of cellular proteolysis. In this system, ubiquitination serves as a targeting signal for proteolysis.[1] Ubiquitin C-terminal hydrolase-L3 (UCH-L3) is one of the components of the ubiquitin–proteasome system and hydrolyzes ubiquitin C-terminal adducts for the recycling of cellular ubiquitin.[2] Ubiquitin with C-terminal adducts is a substrate for UCH-L3, and ubiquitin with a free C-terminus is recycled within the ubiquitin–proteasome system. There is some evidence that UCH-L3 plays an important role in programmed cell death. Programmed cell death is implicated in a number of human diseases, including neurodegenerative disease,[3] autoimmune disease,[4] cancers[5,6], etc. Loss of UCH-L3 leads to programmed cell death by apoptosis of certain type of cells in vivo, germ line cells and photoreceptor cells.[7,8] High-level expression of UCH-L3 genes and proteins, and acceleration of UCH-L3 enzymatic activity is reported in multiple types of cancer cells,[5,6] suggesting that UCH-L3 activity may be required for cancer cell survival. Therefore, UCH-L3 is a potential target for drug development to control programmed cell death in specific types of cells including cancer cells.

Structure-based drug design (SBDD) is a method used to discover novel leads for drug development as it enables more rapid hit identification than the classical screening methods of in vitro or in vivo biological assays. The computer-based approach for drug screening, using molecular docking, is a shortcut method when the crystal structure of a target protein is available. Key methodologies for docking small molecules to protein were developed during the early 1980s,[9] and various types of docking simulation software are now available, for example, DOCK,[10] GOLD, and FlexX.[11] BCR-ABL tyrosine kinase inhibitors (IC_{50} values ranging from 10 to 200 μM) were successfully

Keywords: UCH-L3; Dihydro-pyrrole; Structure-based drug design; Virtual screening.
* Corresponding author. Tel.: +81 42 341 2712x5144; fax: +81 42 346 1745; e-mail: aokis@ncnp.go.jp

0968-0896/$ - see front matter © 2007 Elsevier Ltd. All rights reserved.
doi:10.1016/j.bmc.2007.07.016

identified by virtual screening of 200,000 compounds against crystal structures using DOCK,[12] implemented by the anchor-and-grow algorithm with respect to ligand flexibility.[10] Human thymidine phosphorylase inhibitor (IC_{50} = 77 μM) was also identified by virtual screening of 250,521 compounds using DOCK.[13] Furthermore, metallo-β-lactamase inhibitors (IC_{50} values less than 15 μM) were identified through virtual screening by GOLD,[14] using the genetic algorithm for ligand flexibility.

The advantage of chaining different docking programs was evaluated and the results suggested that virtual ligand screening is performed faster with reasonable accuracy by using chained screening, than by using a single program with default parameters.[15] In this study, the results of chained docking against UCH-L3 crystal structure were examined by UCH-L3 hydrolysis activity assay to validate the efficacy of the DOCK–GOLD SBDD method. We identified three inhibitors (IC_{50} = 100–150 μM) of UCH-L3 by the DOCK–GOLD virtual screening of 32,799 compounds.

2. Results and discussion

2.1. Protein preparation and chemical database

In the 3D structure of the UCH-L3-ubiquitin complex, ubiquitin C-terminus is buried in the active site cleft among four active site residues of UCH-L3: Gln89, Cys95, His169, and Asp184.[16,17] During the virtual screening process by DOCK and GOLD, the protein–ligand interacting site was restricted to the binding site of the three ubiquitin C-terminal amino residues (as described in Section 4), in order that the outcome could be verified by a ubiquitin C-terminal hydrolase enzymatic assay. The first DOCK screening was performed against 32,799 compounds of CNS-Set, which was prefiltered by RPBS under the most modest filtering condition.[18]

2.2. DOCK and GOLD screenings

To screen for compounds that bind to the active site, the first screening was performed by DOCK, and the protein–ligand interaction area was restricted to the ubiquitin binding site of UCH-L3 (see Section 4). The top-scoring 1780 compounds (5.4% of the initial 32,799 compounds) with energy scores of less than −30 kcal/mol were selected for further screening. These compounds were then re-screened by GOLD twice, with different genetic algorithm (GA) settings. To predict binding ability to the active site cleft accurately, the protein–ligand interacting area was defined in approximately the same way as in the first DOCK screening step (see Section 4). Screening by GOLD consisted of two rounds. Using the GOLD score, we initially extracted the top scoring 100 compounds from 1780 compounds, using the 7–8 times speed-up GA parameter settings. These 100 compounds were then re-scored using the default GA settings (see Section 4) to more accurately predict binding ability. Ten compounds with GOLD scores of over 60 were predicted to bind to the UCH-L3 active site; that is, 0.03% of the total number of chemical compounds was screened.

2.3. IC_{50} determination

A previous study demonstrated that compounds with GOLD scores of about 60 may inhibit enzyme activity with IC_{50} values of 10–100 μM.[19] An enzyme assay was performed among the top 10 chemicals to address whether they actually bind to the UCH-L3 active site with the predicted affinities (Table 1 and Fig. 1).

Ubiquitin-7-amido-4-methylcoumarin (Ub-AMC; AMC attaches to the carboxyl terminus of ubiquitin) is a fluorogenic substrate of UCH-L3 and other UCH isozymes. UCH-L3 is known to hydrolyze Ub-AMC into free ubiquitin and AMC,[20,21] and the hydrolyzed AMC group is excited at light wavelength of 355 nm and emits fluorescence at 460 nm. Hydrolysis activity of UCH-L3 is inhibited if a compound binds to its active site and thus blocks interaction between the active site of UCH-L3 and the ubiquitin C-terminus. Inhibition of hydrolysis of Ub-AMC leads to a lower concentration of free AMC and hence a lower level of fluorescence intensity.

We experimentally determined the affinity constant (K_m) of Ub-AMC hydrolysis by human UCH-L3 as 83.3 ± 1.5 nM (mean ± SEM, from three independent experiments). The candidate compounds identified by

Table 1. GOLD scores of the top 10 ranked chemicals after GOLD calculation[a]

Docking rank/Compound No.	Compound name	GOLD scores
1	1-Benzyl-3-hydroxy-4-(5-methyl-2-furoyl)-5-(3-pyridinyl)-1,5-dihydro-2*H*-pyrrol-2-one	66.01
2	3-[4-Methyl-5-({[3-(2-thienyl)-1,2,4-oxadiazol-5-yl]methyl}thio)-4*H*-1,2,4-triazol-3-yl]-1*H*-indole	65.62
3	*N*-{4-[1-(2-Furoyl)-5-(2-furyl)-4,5-dihydro-1*H*-pyrazol-3-yl]phenyl}methanesulfonamide	64.85
4	N^1-Cyclopropyl-N^2-(4-methoxyphenyl)-N^2-[(4-methylphenyl)sulfonyl]glycinamide	64.76
5	*N*-{3-[1-Acetyl-5-(2-thienyl)-4,5-dihydro-1*H*-pyrazol-3-yl]phenyl}ethanesulfonamide	64.23
6	3-Hydroxy-5-(4-methoxyphenyl)-1-(1,3,4-thiadiazol-2-yl)-4-(2-thienylcarbonyl)-1,5-dihydro-2*H*-pyrrol-2-one	62.96
7	5-(4-Fluorophenyl)-3-hydroxy-4-(5-methyl-2-furoyl)-1-(3-pyridinylmethyl)-1,5-dihydro-2*H*-pyrrol-2-one	62.73
8	N^1-Cyclopropyl-N^2-[(4-methoxyphenyl)sulfonyl]-N^2-(4-methylphenyl)glycinamide	62.52
9	N^1-Cyclopentyl-N^2-(3-methoxyphenyl)-N^2-(phenylsulfonyl)glycinamide	62.39
10	4-({[5-(2-Furyl)-4-phenyl-4*H*-1,2,4-triazol-3-yl]thio}methyl)-1,3-thiazol-2-amine	62.35

[a] Ten compounds are listed according to the top 10 rank of GOLD scores and assigned the number corresponding to GOLD score ranks.

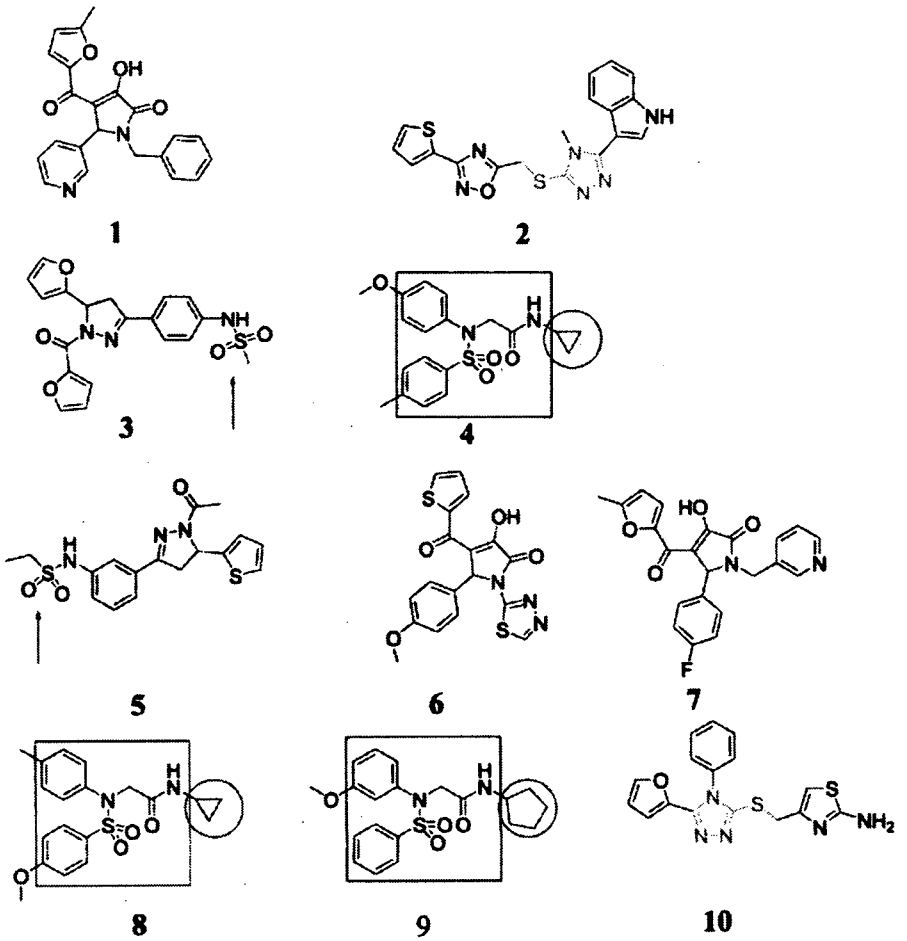

Figure 1. Top 10 ranked compounds identified by DOCK and GOLD screening. Note that there are several shared basic skeletons and functional groups: 1,5-dihydro-2*H*-pyrrol-2-one (drawn in red, compounds **1**, **6**, and **7**), glycinamide (boxed in red, compounds **4**, **8**, and **9**), cycloalkane group (circled in red, compounds **4** and **8**; cyclopropyl, compound **9**; cyclopentyl), 4,5-dihydro-1*H*-pyrazol-3-yl phenyl (drawn in blue, compounds **3** and **5**), sulfonamide (pointed, compounds **3** and **5**), and 4*H*-1,2,4-triazol-3-yl (drawn in green, compounds **2** and **10**).

DOCK–GOLD chained docking screening were tested for their ability to inhibit the hydrolysis activity of UCH-L3, at the Ub-AMC concentration equivalent to the K_m value. Four compounds among these candidates inhibited enzyme activity (Fig. 2a). We did not test the inhibitory effects of compound **3**, as it is a fluorogenic chemical with an emission wavelength of 460 nm. Compounds **1**, **6**, and **7** significantly inhibited the hydrolysis activity of UCH-L3 (initial velocity of Ub-AMC hydrolysis; nM/s [Fig. 2b]). Compounds **1** (401 μM), **6** (375 μM), and **7** (350 μM) inhibited the hydrolysis activity by 83.2 ± 1.5%, 76.5 ± 0.6%, and 76.8 ± 1.0%, respectively, as compared with control DMSO ($p < 0.01$, vs control; Dunnett's test). The IC_{50} value of compound **2** should hypothetically be several hundred μM. Although compound **2** (380 μM) inhibited hydrolysis activity by 16.2 ± 2.1% as compared with control DMSO, the difference was not found to be significant by Dunnett's test. Five other compounds were unable to inhibit the UCH-L3 hydrolysis activity: compound **4** (334 μM; final concentration), compound **5** (331 μM), compound **8** (401 μM), compound **9** (386 μM), and compound **10** (387 μM) (Fig. 2b). Experimentally determined IC_{50} values of compounds **1**, **6**, and **7** (Fig. 3) were as follows: compound **1** (103 μM), compound **6** (154 μM), and compound **7** (123 μM).

2.4. Competitive inhibitor

To show that the identified compounds bind to the active site of the UCH-L3, various concentrations of compound **1** and iodoacetamide (108 mM) were added to UCH-L3/Ub-AMC reaction buffer. Iodoacetamide is a non-competitive inhibitor of UCH-L3 (Fig. 4a). It is a thiol alkylating agent of the UCH-L family and derivatizes and inactivates the active site leading to loss of UCH-L3 enzymatic activity.[22] In the presence of compound **1** and iodoacetamide, the percentage of active UCH-L3 reduced by iodoacetamide treatment was recovered in comparison with the control, and the recovery was dependent on the concentration of compound **1** (Fig. 4b). Our results showed that compound **1** is a competitive inhibitor of UCH-L3. This suggests that compound **1** bound to the UCH-L3 active site to prevent iodoacetamide from inactivating it.

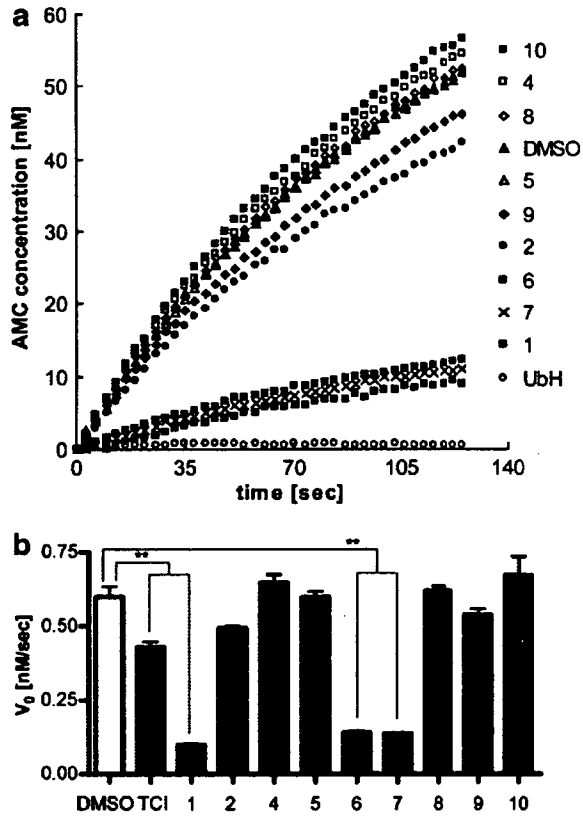

Figure 2. Analysis of UCH-L3 inhibitory effects of compounds 1–10. (a) Kinetics of UCH-L3-catalyzed hydrolysis of Ub-AMC with the compounds. Fluorescence intensity was converted to AMC concentration by subtracting the intensity of fully hydrolyzed substrate from that of solution without substrate. Concentrations of compounds are as follows: compound 1 (401 μM); compound 2 (380 μM); compound 4 (334 μM); compound 5 (331 μM); compound 6 (375 μM); compound 7 (350 μM); compound 8 (401 μM); compound 9 (386 μM); and compound 10 (387 μM). As a known inhibitor, ubiquitin-aldehyde (Ub-H, 120 nM) was used. Each value represents the mean of three independent experiments. (b) Inhibitory effects of compounds on initial velocity of hydrolysis (V_0) are shown. Fluorescence intensity was converted by the same method described in (a). 4,5,6,7-Tetrachloroindan-1,3-dione (TCI, 20 μM) was used as a UCH-L3 selective inhibitor with IC_{50} of 600 nM.[22] Each value represents the mean ± SEM of three independent experiments. Dunnett's multiple comparison test was performed using GraphPad Prism software (**: $p < 0.01$, DMSO as control).[29]

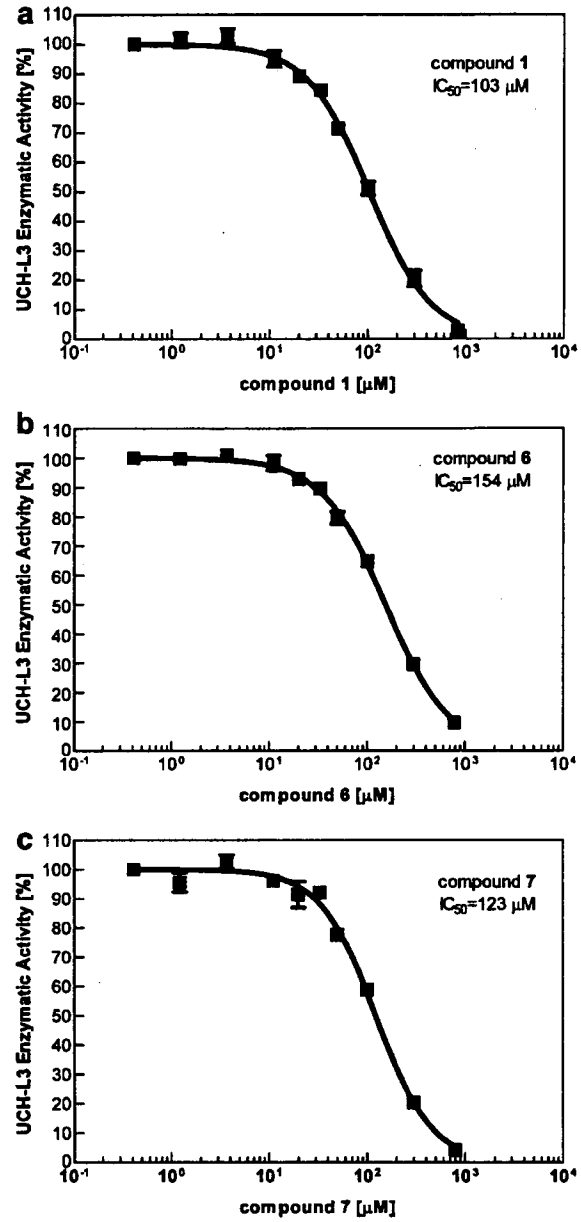

Figure 3. IC_{50} curves of compounds for UCH-L3 enzymatic activity. (a) Compound 1, (b) compound 6, and (c) compound 7. The horizontal axis shows the concentration of each compound. The vertical axis shows the relative UCH-L3 enzymatic activity [%] in comparison with maximal initial velocity. IC_{50} values are shown in graphs. Each plotted value represents the mean ± SEM of three independent experiments.

In order to show that the compounds 1, 6, and 7 bind to UCH-L3, Biacore 100 analysis was conducted. Biacore 100 analysis detects interaction between a small molecule and protein and enables quantification of the interaction.[23] The results showed that binding of each compound to UCH-L3 increased and was dependent on the concentration of the compound 6 (data not shown).

2.5. Predicted binding mode

Figure 5 shows the predicted binding modes of compounds 1, 6, and 7 to UCH-L3. Since chemical formulae of the three compounds are similar to each other, the predicted docked structures of these and UCH-L3 have similar binding modes. Two hydrogen bonds were observed between the docked ligand and two amino acid residues in the predicted compound 1/UCH-L3 complex structure; the carbonyl group of compound 1 appears to form a hydrogen bond to the NH group of Ala11, and the pyrrole C=O appears to form a hydrogen bond to the hydroxyl group of Thr157. Three hydrogen bonds were predicted between the docked ligand and two amino acid residues in the compound 6/UCH-L3 complex structure; the thiadiazole group of compound 6 appears to form a hydrogen bond to the NH group of Leu9, and

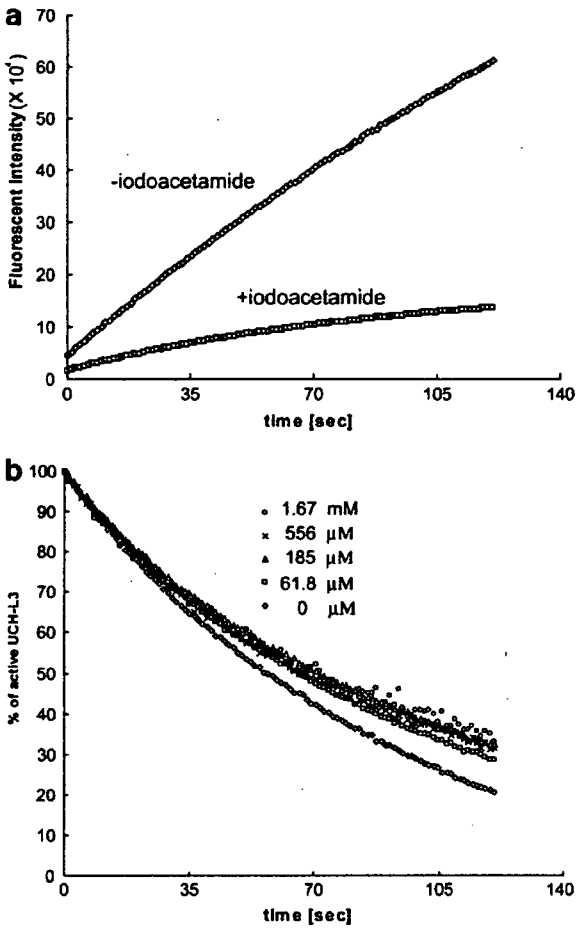

Figure 4. Competitive inhibition of compound 1. (a) Kinetics of UCH-L3-catalyzed hydrolysis of Ub-AMC with or without iodoacetamide (108 mM). (b) Reaction progress curves normalized by final fluorescence intensity representing the ratio of active UCH-L3 (for calculations, see Section 4.9), in the presence of iodoacetamide (108 mM) and compound 1 (0 μM, 61.8 μM, 185 μM, 556 μM, and 1.67 mM).

the pyrrole hydroxyl group and pyrrole C=O appear to form a hydrogen bond to the NH group of Ala11. A hydrogen bond was observed between the docked ligand and the amino acid residues of UCH-L3 in the predicted compound 7/UCH-L3 complex structure; the carbonyl group of compound 7 appears to form a hydrogen bond to the NH group of Ala11. The predicted binding mode of compound 10, as a non-binder, was analyzed. Four hydrogen bonds were observed between the docked ligand and the amino acid residues of UCH-L3 in the predicted compound 10/UCH-L3 complex structure. The triazol group of compound 10 appears to form two hydrogen bonds to the hydroxyl group of Thr157, and the amino group of compound 10 appears to form a hydrogen bond to the CO group of Glu154, and to the CO group of Ser151. Although hydrogen bonds between actual inhibitors (compounds 1, 6, and 7) and Ala11 were observed, compound 10, a non-inhibitor, does not appear to form a hydrogen bond to Ala11. This hydrogen bond might be important for compounds to bind stably to the UCH-L3 active site.

2.6. Discussion; analysis of active compounds

By three-step virtual screening (DOCK, high-speed GOLD, and low-speed GOLD) of 32,799 chemicals, we identified 10 candidate chemicals that potentially inhibit UCH-L3 hydrolysis activity. We examined the actual inhibitory effects of the compounds on UCH-L3 hydrolysis activity by biochemical enzymatic assay and identified three compounds (compounds 1, 6, and 7) as UCH-L3 inhibitors, with IC_{50} values of 100–150 μM. By comparing the structural formulae of the three compounds, we found that the 1,5-dihydro-2*H*-pyrrol-2-one group is likely to be important for inhibition of UCH-L3-hydrolysis activity (Fig. 6). Several common structural features can be drawn from these three chemicals (Fig. 6). First, the heteroaromatic pyrrole group is common to all three compounds. Second, each of the three compounds also contains pyridines and furoyls as heteroaromatic functional groups. Third, a carbon–oxygen double bond at position 2, a hydroxyl group at position 3, a carbonyl group at position 4, and a hydrogen atom at position 5 of the pyrrole ring are common to each compound. Fourth, a five- or six-membered cyclic group at positions 1, 4, and 5 is common to all three chemicals (Fig. 6). Furthermore, compounds 1 and 7 have two heteroaromatic groups: a pyridinyl group and a furoyl group.

The structural similarities of UCH-L3-binding chemicals have an influence on binding mode similarities. There are two main pockets in the substrate-binding site of UCH-L3: the first pocket (Pocket 1) is formed by Pro8, Glu10, and Thr157 and the second pocket (Pocket 2), the active site pocket, is formed by Asp167, Leu168, and Cys90. Docked orientations of compounds 1 and 7 are very similar, as positions 1 and 5 six-membered cyclic groups fit into each pocket. This suggests that two features among these similarities are likely to be important for stable binding to the active site: a pyrrole ring and two heteroaromatic groups, which fit into both pockets around the UCH-L3 substrate-binding site. The shape of Pocket 1 is different from that of UCH-L1,[24] another isoform of the UCH family (52% amino acid sequence identity).[25] Thus, modification of the chemical groups in Pocket 1 might be effective during drug design, to enhance specificity for UCH-L3 over UCH-L1.

Several lines of evidence indicate that UCH-L3 is associated with tumorigenesis and carcinogenesis. High-level expression and activity of UCH-L3 has been reported in multiple types of cancer cells. Expression of UCH-L3 mRNA is upregulated in breast tumors and UCH-L3 mRNA levels are associated with the histological grading of such tumors.[5] Moreover, it has been suggested that the activity of UCH-L3 is also upregulated in the majority of cervical carcinoma tissues, compared with adjacent normal tissues.[6] On the other hand, loss of UCH-L3 is known to induce cell death in knock-out studies. UCH-L3 is involved in the protection of programmed cell death in germ cells and photoreceptor cells in vivo.[7,8] Thus, the structural information of the

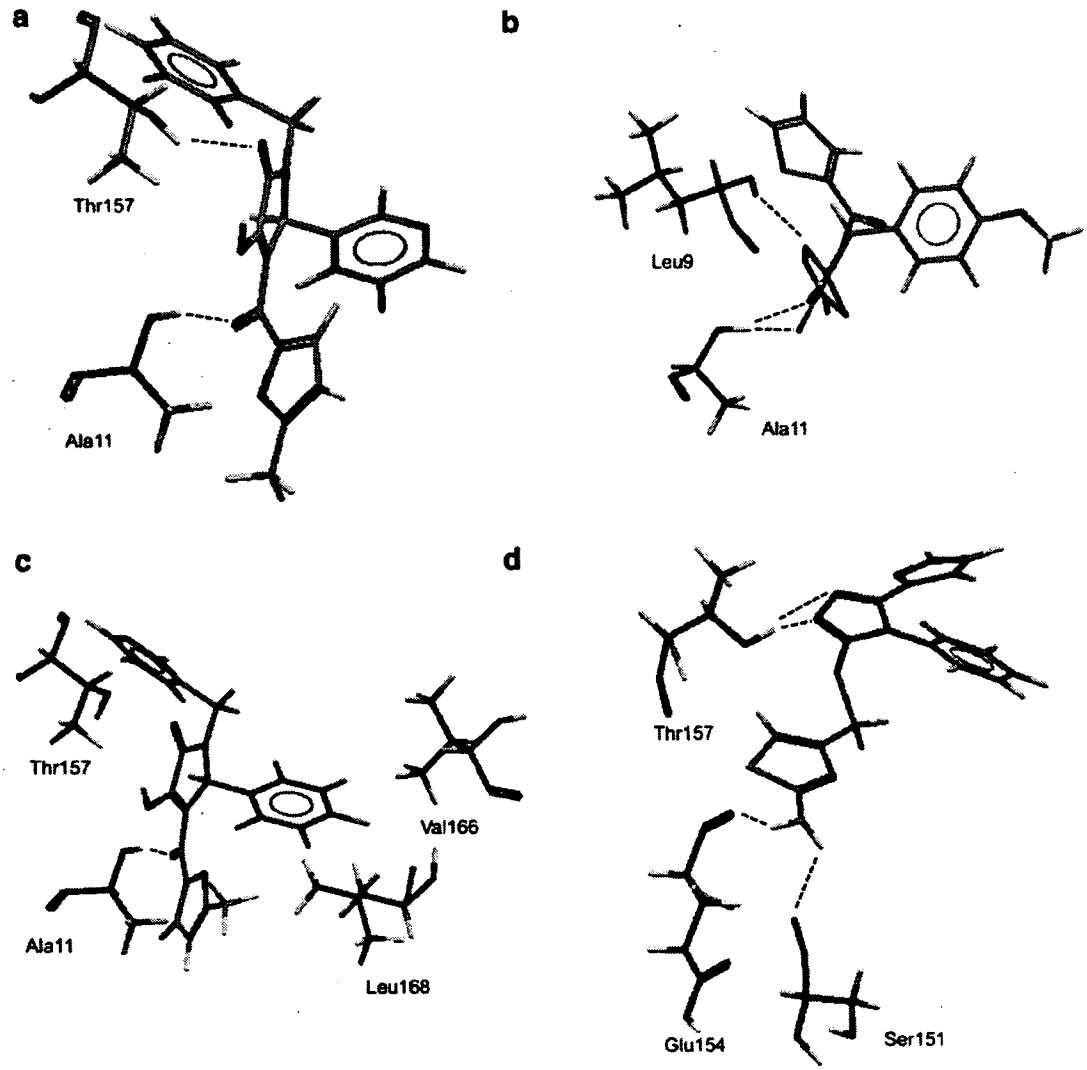

Figure 5. Illustration showing the molecular docking results. Docked orientation of (a) compound **1**, (b) compound **6**, (c) compound **7**, and (d) compound **10** in the UCH-L3 active site using GOLD and shown with interacting residues. Hydrogen bonds are shown by a dashed line. Oxygen atoms are shown in red, nitrogen atoms in blue, sulfur atoms in orange, fluorine atoms in yellow, and hydrogen atoms in gray. The enzyme carbons are shown in dark gray and those of the ligands in green.

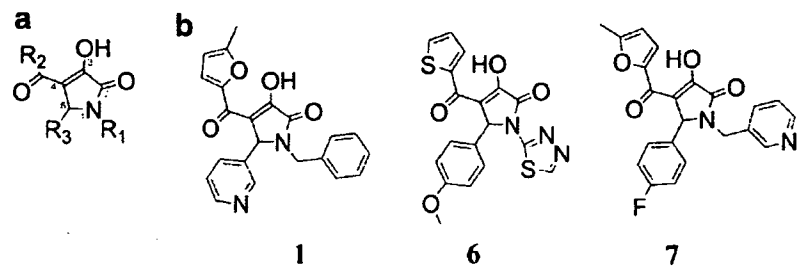

Figure 6. Structural similarities of the three compounds. (a) 1,5-Dihydro-2*H*-pyrrol-2-one group, the common basic skeleton, is shown in red. Position numbers of the pyrrole ring are shown as small characters. R_1–R_3 represent each functional group at positions 1, 4, and 5 of the pyrrole ring, respectively. (b) Structures of identified inhibitors: compounds **1**, **6**, and **7**.

UCH-L3 inhibitors we identified may be useful for future apoptosis-inducing anti-cancer drug development. UCH-L3 should be an important target for modulating cell apoptosis.

3. Conclusion

In this study, we employed three-step docking (DOCK, rough GOLD, and fine GOLD) and in vitro enzyme

assay methods, and identified three UCH-L3 inhibitors with IC_{50} values of 100–150 μM. These novel inhibitors have a dihydro-pyrrole group in common.

4. Experimental

4.1. Compound library

We used the ADME/Tox (absorption, distribution, metabolism, excretion, and toxicity) filtered virtual compound library (ChemBridge CNS-Set) which includes a collection of 32,799 chemical compounds.[18] All compounds satisfy Lipinski's Rule of five.

4.2. Protein preparation

Human UCH-L3 and ubiquitin vinylmethylester (Ub-VME) complex crystal structure data (PDB code; 1XD3) were obtained from Protein Data Bank (PDB).[17] Hydrogens were added to UCH-L3-ubiquitin complex using CVFF99 force field by Biopolymer module in Insight II 2000 suite (Accelrys, Inc., San Diego, CA). Energy was minimized by the Discover 3 module of the same suite with all heavy atoms restrained, except hydrogen, to relieve any short contacts. To use the UCH-L3 protein structure in the following docking simulations, the structures of UCH-L3 and Ub-VME complex were divided into their components.

4.3. Virtual screening

Virtual screening experiments were performed by UCSF DOCK 5.4.0[10] and GOLD 3.0.1 (CCDC, Cambridge, UK).[26] In the first screening by DOCK, the substrate-binding site was defined, by selecting ligand atom accessible spheres and describing molecular surfaces with the SPHERE_GENERATOR program in the DOCK suite. All spheres within 6 Å of root mean square deviation (RMSD) from every atom of the three C-terminal residues of energy-minimized ubiquitin were selected by the SPHERE_SELECTOR program in DOCK suite. A scoring function ($E_{int} = E_{vdw} + E_{elec}$) was used to estimate potential binding affinity. Following the first screening with rigid ligand conditions, 1780 compounds with binding energy scores of less than −30 kcal/mol were selected for a second screening by GOLD.

Using GOLD, the 1780 compounds were screened with 7–8 times speed-up settings; that is, the pre-defined genetic algorithm (GA) parameter settings to achieve calculation speed-up. The top-ranked 100 compounds were determined, then screened by default settings; the GA parameter settings for a slower calculation with greater ligand flexibility, but with a more accurate prediction. Ligand flexibility was turned on in both the 7–8 times speed-up settings and the default settings. Protein side chain flexibility was not turned on in any settings. The virtual tripeptide structure composed of three C-terminal residues of the energy-minimized ubiquitin was set as the reference ligand to define the ligand-binding site. All protein atoms within 5 Å of each ligand atom were used for defining the binding site. The solvent-accessible surfaces of the docking region were restricted by a cavity detection algorithm.[27] As a result, the binding site was composed of 174 active atoms (automatically selected by GOLD software). A method for defining the binding site with tripeptide yielded the best score among other methods using shorter or longer C-terminal peptide sequences of ubiquitin (data not shown). Ten docking solutions for each docked molecule were scored and the top three were saved for post-screening evaluations. Potential hydrogen bonds and van der Waals contacts were identified using Silver 1.0 (CCDC, Cambridge, UK).[28] Ligands predicted to be tight-binders by both DOCK and GOLD were applied to further in vitro experimental validation. All calculations were performed on seven Linux or Cygwin 2–3 GHz/Pentium IV CPU personal computers.

4.4. Statistical analysis

All statistical analysis was performed by GraphPad Prism 4 (GraphPad Software, Inc., San Diego, CA).[29]

4.5. Reagents

Human recombinant UCH-L3, ubiquitin-7-amido-4-methylcoumarin (Ub-AMC), and ubiquitin-aldehyde (Ub-H) were purchased from Boston Biochem, Inc. (Cambridge, MA). 4,5,6,7-Tetrachloroindan-1,3-dione (TCI) was purchased from Fisher Scientific International Inc. (Hampton, NH). Iodoacetamide was purchased from Sigma–Aldrich Corporation (St. Louis, MO). Compounds within ChemBridge CNS-Set (Supplier IDs given in parentheses) are as follows: compound **1**: 1-benzyl-3-hydroxy-4-(5-methyl-2-furoyl)-5-(3-pyridinyl)-1,5-dihydro-2*H*-pyrrol-2-one (7504601); compound **2**: 3-[4-methyl-5-({[3-(2-thienyl)-1,2,4-oxadiazol-5-yl]methyl}thio)-4*H*-1, 2,4-triazol-3-yl]-1*H*-indole (7950509); compound **3**: *N*-{4-[1-(2-furoyl)-5-(2-furyl)-4,5-dihydro-1*H*-pyrazol-3-yl]phenyl}methanesulfonamide (7977303); compound **4**: N^1-cyclopropyl-N^2-(4-methoxyphenyl)-N^2-[(4- methylphenyl)sulfonyl]glycinamide (6382507); compound **5**: *N*-{3-[1-acetyl-5-(2-thienyl)-4,5-dihydro-1*H*-pyrazol-3-yl]phenyl}ethanesulfonamide (7909542); compound **6**: 3-hydroxy-5-(4-methoxyphenyl)-1-(1,3,4-thiadiazol-2-yl)-4-(2-thienylcarbonyl)-1,5-dihydro-2*H*-pyrrol-2-one (6237842); compound **7**: 5-(4-fluorophenyl)-3-hydroxy-4-(5-methyl-2-furoyl)-1-(3-pyridinylmethyl)-1,5-dihydro-2*H*-pyrrol-2-one (6771097); compound **8**: N^1-cyclopropyl-N^2-[(4-methoxyphenyl)sulfonyl]-N^2-(4-methylphenyl)glycinamide (6699002); compound **9**: N^1-cyclopentyl-N^2-(3-methoxyphenyl)-N^2-(phenylsulfonyl)glycinamide (6187162); and compound **10**: 4-({[5-(2-furyl)-4-phenyl-4*H*-1,2,4-triazol-3-yl]thio}methyl)-1,3-thiazol-2-amine (9012750) were purchased from ChemBridge Corporation (San Diego, CA).

4.6. Enzymatic assay

UCH-L3 activity was assayed using modification of a technique described in previous studies.[22,30] The enzyme

reactions were carried out at a final volume of 205 μl on Costar 96-well black assay plates (part number 3915, Corning Inc., Corning, NY). Then, 5 μl of solution containing each compound (100% DMSO), or 5 μl of 100% DMSO as a negative control, was added to 100 μl of enzyme buffer solution (50 pM of UCH-L3, 20 mM Hepes [pH 7.8], 0.5 mM EDTA, 5 mM dithiothreitol [DTT], and 0.1 mg/ml ovalbumin) in each well. The solution was incubated for 30 min at room temperature. To start the enzyme reaction, 100 μl of substrate buffer solution (82 nM of ubiquitin-AMC, 20 mM Hepes [pH 7.8], 0.5 mM EDTA, 5 mM DTT, and 0.1 mg/ml ovalbumin) was added to each well. AMC fluorescence (excitation wavelength: 355 nm, emission wavelength: 460 nm) was subsequently measured 40 times every 3 s with a Wallac 1420 multi-label counter (Perkin-Elmer, Wellesley, MA).

4.7. K_m determination

Fifty microliters of enzyme buffer solution was added to each plate well. The solution was incubated for 30 min at room temperature. To start the enzyme reaction, 50 μl of substrate buffer solution (23.1, 46.3, 92.5, 185, 370, and 740 nM of ubiquitin-AMC; the concentrations of other components were as described previously) was added to each well. Fluorescence of AMC was measured 40 times every 3 s with the Wallac multi-label counter. Initial velocities (from 0 to 30 s) were used for K_m determination, using GraphPad Prism 4 software.[29]

4.8. Experimental IC_{50} determination

Five microliters of solution containing each compound (0.412 μM, 1.23, 3.70, 11.1, 20, 33.3, 50, 100, 300, and 700–850 μM) or 5 μl of 100% DMSO (as a negative control) diluted in 100 μl of enzyme buffer solution was added to each plate well. This solution was incubated for 30 min at room temperature. To start the enzyme reaction, 100 μl of substrate buffer solution was added to each well. Fluorescence of AMC was measured 40 times every 3 s with the Wallac multi-label counter. Initial velocities (from 0 to 30 s) were used for IC_{50} determination, using GraphPad Prism 4 software.[29]

4.9. Active site binding experiment

Modification of a technique described in previous studies was used to determine whether or not the compounds bind to the active site.[22] Five microliters of solution containing compound 1 (0 μM, 61.8 μM, 185 μM, 556 μM, and 1.67 mM) or 5 μl of 100% DMSO (as a negative control) diluted in 80 μl of enzyme buffer solution (UCH-L3: 1 nM) was added to each plate well. This solution was incubated for 30 min at room temperature. To start the enzyme reaction, 80 μl of substrate buffer solution (Ub-AMC: 1 μM) was added to each well, followed within 2 s by addition of 40 μl of iodoacetamide (108 mM) or water as a negative control. Fluorescence of AMC was measured 100 times every second using the Wallac multi-label counter. The percentage of active site survival $[(F_{saturated} - F_t)/(F_{saturated} - F_{t=0}) \times 100]$ was calculated.

Acknowledgments

This work was supported by Grants-in-Aid for Scientific Research from the Ministry of Health, Labour and Welfare of Japan, Grants-in-Aid for Scientific Research from the Ministry of Education, Culture, Sports, Science and Technology of Japan, a grant from the Program for Promotion of Fundamental Studies in Health Sciences of the National Institute of Biomedical Innovation, a grant from Japan Science and Technology Cooperation, and a grant from New Energy and Industrial Technology Development Organization. We thank Takashi Kaburagi for demonstrating how to set up the DOCK software.

References and notes

1. Ciechanover, A.; Schwartz, A. L. *Proc. Natl. Acad. Sci. U.S.A.* **1998**, *95*, 2727–2730.
2. Pickart, C. M.; Rose, I. A. *J. Biol. Chem.* **1985**, *260*, 7903–7910.
3. Waldmeier, P.; Bozyczko-Coyne, D.; Williams, M.; Vaught, J. L. *Biochem. Pharmacol.* **2006**, *72*, 1197–1206.
4. Aktas, O.; Waiczies, S.; Zipp, F. *J. Neuroimmunol.* **2007**, *184*, 17–26.
5. Miyoshi, Y.; Nakayama, S.; Torikoshi, Y.; Tanaka, S.; Ishihara, H.; Taguchi, T.; Tamaki, Y.; Noguchi, S. *Cancer Sci.* **2006**, *97*, 523–529.
6. Rolen, U.; Kobzeva, V.; Gasparjan, N.; Ovaa, H.; Winberg, G.; Kisseljov, F.; Masucci, M. G. *Mol. Carcinog.* **2006**, *45*, 260–269.
7. Kwon, J.; Wang, Y. L.; Setsuie, R.; Sekiguchi, S.; Sato, Y.; Sakurai, M.; Noda, M.; Aoki, S.; Yoshikawa, Y.; Wada, K. *Am. J. Pathol.* **2004**, *165*, 1367–1374.
8. Sano, Y.; Furuta, A.; Setsuie, R.; Kikuchi, H.; Wang, Y. L.; Sakurai, M.; Kwon, J.; Noda, M.; Wada, K. *Am. J. Pathol.* **2006**, *169*, 132–141.
9. Kuntz, I. D.; Blaney, J. M.; Oatley, S. J.; Langridge, R.; Ferrin, T. E. *J. Mol. Biol.* **1982**, *161*, 269–288.
10. Ewing, T. J.; Makino, S.; Skillman, A. G.; Kuntz, I. D. *J. Comput. Aided Mol. Des.* **2001**, *15*, 411–428.
11. FlexX, BioSolveIT GmbH, Sankt Augustin, Germany, <http://www.biosolveit.de/>.
12. Peng, H.; Huang, N.; Qi, J.; Xie, P.; Xu, C.; Wang, J.; Yang, C. *Bioorg. Med. Chem. Lett.* **2003**, *13*, 3693–3699.
13. McNally, V. A.; Gbaj, A.; Douglas, K. T.; Stratford, I. J.; Jaffar, M.; Freeman, S.; Bryce, R. A. *Bioorg. Med. Chem. Lett.* **2003**, *13*, 3705–3709.
14. Olsen, L.; Jost, S.; Adolph, H. W.; Pettersson, I.; Hemmingsen, L.; Jorgensen, F. S. *Bioorg. Med. Chem.* **2006**, *14*, 2627–2635.
15. Miteva, M. A.; Lee, W. H.; Montes, M. O.; Villoutreix, B. O. *J. Med. Chem.* **2005**, *48*, 6012–6022.
16. Johnston, S. C.; Larsen, C. N.; Cook, W. J.; Wilkinson, K. D.; Hill, C. P. *EMBO J.* **1997**, *16*, 3787–3796.
17. Misaghi, S.; Galardy, P. J.; Meester, W. J.; Ovaa, H.; Ploegh, H. L.; Gaudet, R. *J. Biol. Chem.* **2005**, *280*, 1512–1520.
18. RPBS, Paris, France, <http://bioserv.rpbs.jussieu.fr/RPBS/cgi-bin/Ressource.cgi?chzn_lg=an&chzn_rsrc=Collections/>.
19. GOLD User Guide, 16.2.1, CCDC, Cambridge, UK, <http://www.ccdc.cam.ac.uk/support/documentation/gold/3_1/gold31.pdf/>.
20. Dang, L. C.; Melandri, F. D.; Stein, R. L. *Biochemistry* **1998**, *37*, 1868–1879.

21. Mason, D. E.; Ek, J.; Peters, E. C.; Harris, J. L. *Biochemistry* **2004**, *43*, 6535–6544.
22. Liu, Y.; Lashuel, H. A.; Choi, S.; Xing, X.; Case, A.; Ni, J.; Yeh, L. A.; Cuny, G. D.; Stein, R. L.; Lansbury, P. T., Jr. *Chem. Biol.* **2003**, *10*, 837–846.
23. Stenlund, P.; Frostell-Karlsson, A.; Karlsson, O. P. *Anal. Biochem.* **2006**, *353*, 217–225.
24. Das, C.; Hoang, Q. Q.; Kreinbring, C. A.; Luchansky, S. J.; Meray, R. K.; Ray, S. S.; Lansbury, P. T.; Ringe, D.; Petsko, G. A. *Proc. Natl. Acad. Sci. U.S.A.* **2006**, *103*, 4675–4680.
25. Kurihara, L. J.; Semenova, E.; Levorse, J. M.; Tilghman, S. M. *Mol. Cell. Biol.* **2000**, *20*, 2498–2504.
26. Jones, G.; Willett, P.; Glen, R. C.; Leach, A. R.; Taylor, R. *J. Mol. Biol.* **1997**, *267*, 727–748.
27. Hendlich, M.; Rippmann, F.; Barnickel, G. *J. Mol. Graph. Model.* **1997**, *15*, 359–363.
28. Silver, CCDC, Cambridge, UK, <http://www.ccdc.cam.ac.uk/>.
29. GraphPad Prism 4, GraphPad Software, San Diego, CA, <http://www.graphpad.com/www/about.htm/>.
30. Nishikawa, K.; Li, H.; Kawamura, R.; Osaka, H.; Wang, Y. L.; Hara, Y.; Hirokawa, T.; Manago, Y.; Amano, T.; Noda, M.; Aoki, S.; Wada, K. *Biochem. Biophys. Res. Commun.* **2003**, *304*, 176–183.

3, respectively). To determine whether the difference in locomotor activity on day 1 was due to reduced exploratory behaviour in *gad* mice, we measured the frequency of rearing, a typical exploratory behaviour (Lever *et al.*, 2006; Fig. 2E). Similar to locomotor activity, upon re-exposure rearing frequency decreased in wild-type mice ($P = 0.009$, $F = 14.257$, $n = 7$; repeated-measures ANOVA) but not in *gad* mice ($P = 0.131$, $F = 2.503$, $n = 6$; repeated-measures ANOVA). The rearing frequency on days 1 and 2 differed significantly between wild-type and *gad* mice ($P = 0.014$ and 0.021 for days 1 and 2, respectively; two-tailed Student's *t*-test), but the activity on day 3 did not ($P = 0.093$). These results suggest that exploratory behaviour in a novel environment is reduced in *gad* mice.

Although these data apparently suggest that memory in passive avoidance learning and exploratory behaviour are reduced in young *gad* mice, there is a possibility that the anxiety state of *gad* mice is altered. Alterations in the anxiety state can affect memory (Bouton *et al.*, 1990) and the response to novel environments. To measure anxiety, we performed a light–dark box test. In this test, mice usually avoid the light compartment. Therefore, the level of anxiety can be measured as the latency to move into the light compartment and the duration of time in the light compartment (Yamada *et al.*, 2002). Because the passive avoidance test also utilizes these properties, performance in the light–dark test is important for interpreting the results from the passive avoidance test. The time required for the mice to step into the light compartment when introduced into the dark compartment (dark-light latency; Fig. 3A), the time the mice spent in the light compartment (Fig. 3A) and the number of times the mice crossed between compartments (Fig. 3B) did not differ significantly between wild-type and *gad* mice ($P = 0.834$, 0.417 and 0.109, respectively; two-tailed Student's *t*-test). These results suggest that anxiety state, as assessed by this test, was not obviously altered in *gad* mice. Therefore we concluded that the impairments in passive avoidance learning and exploratory behaviour were not due to alterations in the anxiety state.

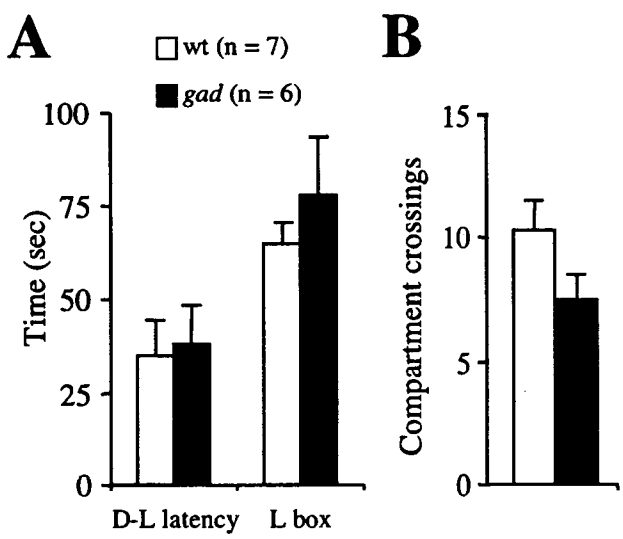

FIG. 3. Wild-type and *gad* mice performed similarly in the light–dark box test. (A) Dark–light (D-L) latency and duration of time in the light compartment (L box). (B) Number of crossings between the two compartments.

Impairment of a transcription-dependent component of LTP in gad mice

We tested whether the lack of UCH-L1 affects neuronal function by measuring LTP at Schaffer collateral synapses onto CA1 pyramidal neurons in hippocampal slice preparations. LTP is believed to be a synaptic mechanism underlying memory and learning (Bliss & Collingridge, 1993). The CA1 synapse was selected because this brain region is involved in spatial memory (Morris *et al.*, 1982) and passive avoidance memory (Bevilaqua *et al.*, 1997; Impey *et al.*, 1998). In wild-type slices, TBS induced robust LTP at CA1 synapses (Fig. 4A), as reported for C57BL/6J mice (Nguyen & Kandel, 1997; Nguyen *et al.*, 2000). In contrast, TBS-induced LTP was attenuated in *gad* mice beginning ~20 min post-TBS (Fig. 4A). At 45 min post-TBS, normalized synaptic responses were significantly greater in wild-type slices (1.87 ± 0.08, $n = 7$) than in *gad* slices (1.36 ± 0.07, $n = 6$; $P = 0.001$, two-tailed Student's *t*-test). Impairment of LTP in *gad* mice depended on the stimulation pattern. Tetanus-induced LTP was identical in wild-type and *gad* mice (Fig. 4B; normalized fEPSP slopes at 45 min post-tetanus: wild-type, 1.81 ± 0.16, $n = 5$; *gad*, 1.86 ± 0.25, $n = 5$).

Stimulus–output curves (Fig. 5A) and paired-pulse facilitation (Fig. 5B) of CA1 synapses were essentially identical in wild-type and *gad* mice. The latter result suggests that a postsynaptic, rather than presynaptic, mechanism is involved in impairment of TBS-induced LTP in *gad* mice. LTP at this synapse is dependent on postsynaptic NMDA receptors (Harris *et al.*, 1984; Larson & Lynch, 1988). Therefore, we tested whether NMDA receptor activity was reduced in *gad* mice using patch-clamp recordings. For this purpose, we recorded Schaffer collateral–CA1 synaptic responses in neurons voltage-clamped to −70 and +40 mV in the presence of picrotoxin (50 μM). The amplitude of the synaptic response recorded at +40 mV at 100 ms poststimulation was normalized to the peak amplitude of the response at −70 mV to estimate the ratio of NMDA-mediated to non-NMDA-mediated currents (Fig. 5D). Because superfusion of the slices with picrotoxin frequently elicited epileptiform activity (data not shown), three to five synaptic responses without epileptiform activity were selected and averaged. The ratio was identical in wild-type and *gad* mice (0.45 ± 0.05, $n = 5$ and 0.43 ± 0.05, $n = 7$ for wild-type and *gad* mice, respectively; two-tailed Student's *t*-test). Therefore, attenuation of synaptic NMDA receptor activity does not account for reduced LTP in *gad* mice. Resting membrane potential and input resistance of CA1 pyramidal neurons did not differ substantially between wild-type and *gad* mice [resting membrane potential, -60.1 ± 0.4 mV for wild-type mice ($n = 20$) and -60.0 ± 0.6 mV for *gad* mice ($n = 20$); input resistance, 163 ± 9.6 for wild-type mice ($n = 16$) and 175 ± 10.8 for *gad* mice ($n = 13$); results obtained from the records using potassium-gluconate pipette solution].

CA1 LTP is composed of early and late temporal phases (Nguyen *et al.*, 1994; Abel *et al.*, 1997; Nguyen & Kandel, 1997). The former is induced mainly by an increase in the number of AMPA-type glutamate receptors at the synapse (reviewed in Malinow & Malenka, 2002) whereas the latter is induced by new protein synthesis from transcription of new mRNA (Nguyen *et al.*, 1994) and/or local protein synthesis from previously expressed mRNA (Bradshaw *et al.*, 2003). Because no obvious changes in the early phase of LTP (up to ~20 min post-TBS) were observed in *gad* mice, we tested whether the late phase is occluded in *gad* mice. For this purpose, we applied actinomycin D, a transcription inhibitor, to the slices and compared suppression of TBS-induced LTP in wild-type and *gad* mice. In wild-type mice, the maintenance of TBS-induced LTP was suppressed by actinomycin D (Fig. 6A). The normalized fEPSP slope at 45 min

Available online at www.sciencedirect.com
ScienceDirect
European Journal of Pharmacology 573 (2007) 20–28
www.elsevier.com/locate/ejphar

Alpha 1-adrenoceptor agonists protect against stress-induced death of neural progenitor cells

Hiroki Ohashi [a,b], Kaori Nishikawa [a,c], Koichi Ayukawa [a,d], Yoko Hara [a], Mika Nishimoto [a,e], Yoshihisa Kudo [e], Toshiaki Abe [b], Shunsuke Aoki [a,c,f,*], Keiji Wada [a,f]

[a] *Department of Degenerative Neurological Diseases, National Institute of Neuroscience, NCNP, Kodaira, Tokyo 187-8502, Japan*
[b] *Department of Neurosurgery, Jikei University Graduate School of Medicine, Minatoku, Tokyo 105-8401, Japan*
[c] *NEDO (New Energy and Industrial Technology Development Organization), Kawasaki, Kanagawa 212-8554, Japan*
[d] *Japan Society for the Promotion of Science (JSPS), Chiyodaku, Tokyo 102-8471, Japan*
[e] *Laboratory of Cellular Neurobiology, Tokyo University of Pharmacy and Life Science, Hachioji, Tokyo 192-0392, Japan*
[f] *CREST (Core Research for Evolutional Science and Technology) of Japan Science and Technology Corporation (JST), Kawaguchi, Saitama 332-0012, Japan*

Received 15 February 2007; received in revised form 18 June 2007; accepted 26 June 2007
Available online 12 July 2007

Abstract

Here, we show that α_1-adrenoceptor agonists suppress stress-induced death of mouse embryonic brain-derived neural progenitor cells (NPCs). NPCs highly expressed both α_{1A}- and α_{1B}-adrenoceptor genes, whereas the gene encoding α_{1D}-adrenoceptor was expressed at low levels. Application of the α_1-adrenoceptor agonists phenylephrine and cirazoline significantly promoted cell survival of embryonic NPCs that had been exposed to stress, as measured by a lactate dehydrogenase release assay, but had no remarkable effect on differentiation of the NPCs. Both phenylephrine and cirazoline protected NPCs from death induced by growth factor deprivation, N2 nutrient deprivation, tunicamycin treatment or staurosporine treatment. Phenylephrine and cirazoline treatments both maximally reduced stress-induced cell death by ~60% but did not change the percentage of undifferentiated cells as measured by nestin staining. Moreover, phenylephrine and cirazoline treatments did not affect the cellular activities of caspase-3 and caspase-7 but markedly reduced propidium iodide penetration into the cytoplasm, suggesting that α_1-adrenoceptor agonists inhibit caspase-3/7-independent death of the embryonic NPCs.

Keywords: α_1-adrenoceptor; GPCR; Neural progenitor cell; Cell death; Cell stress; Phenylephrine; Cirazoline

1. Introduction

The noradrenergic system is proposed to play multiple roles in the adult central nervous system (CNS). Apart from its classical transmitter signaling action, noradrenaline has important roles in attention, arousal, and memory reviewed in Murchison et al., (2004); Southwick et al., (1999). Furthermore, it was proposed that noradrenaline influences the survival, maintenance and plasticity of CNS neurons, including the regulation of endogenous neurotrophin systems, glial function, CNS energy utilization and extracellular homeostasis, and has anti-inflammatory and anti-oxidant effects reviewed in Marien et al., (2004). All cell surface adrenoceptors are members of the G protein-coupled receptor family and mediate responses to extracellular noradrenaline. To date, three subfamilies of adrenoceptors (α_1, α_2 and β) have been identified (Bylund et al., 1995). The adrenoceptors are expressed in many tissues, particularly in the cardiovascular, genitourinary and nervous systems. High levels of adrenoceptors are also present in the neocortex during embryogenesis (Lidow and Rakic, 1992), and there are regional concentrations of α_1, α_2, and β adrenoceptors in the fetal forebrain (Lidow and Rakic, 1994). There are three subtypes of α_1-adrenoceptors, the α_{1A}, α_{1B}, α_{1D}-adrenoceptor, with varying degrees of efficiency of G protein (Gq/11) coupling ($\alpha_{1A}>\alpha_{1B}>\alpha_{1D}$ adrenoceptor) reviewed in Hieble et al., (1995). This leads to activation of downstream signal

* Corresponding author. Department of Degenerative Neurological Diseases, National Institute of Neuroscience, National Center of Neurology and Psychiatry, 4-1-1 Ogawahigashi, Kodaira, Tokyo 187-8502, Japan. Tel.: +81 42 346 1715; fax: +81 42 346 1745.
E-mail address: aokis@ncnp.go.jp (S. Aoki).

0014-2999/$ - see front matter © 2007 Elsevier B.V. All rights reserved.
doi:10.1016/j.ejphar.2007.06.060

transduction pathways, including Ca^{2+}, arachidonic acid, phospholipase C and phospholipase D signals reviewed in Zhong and Minneman (1999). α_1-adrenoceptors are specifically localized to NPCs located in the ventricular zone and subventricular zone in the embryonic rat forebrain, and noradrenaline-containing fibers are also present in both the ventricular zone and subventricular zone (Pabbathi et al., 1997). In addition, noradrenaline has been suggested to regulate development of the murine forebrain. The β-adrenoceptor agonist isoproterenol alters proliferation and differentiation of neural precursors in the cerebral cortex (Slotkin et al., 1988). α_1-adrenoceptors were also implicated in controlling cell proliferation and survival in a rat cortical mixed cell culture and in a heterochronic coculture system of the rat neocortex and rostral pons (Pabbathi et al., 1997; Popovik and Haynes, 2000). Although the functions of α_1-adrenoceptors in the mixed-culture NPCs and in the organ culture were investigated, the function of α_1-adrenoceptors and the direct effects of α_1-adrenoceptor-selective agonists such as phenylephrine and cirazoline in isolated pure embryonic NPCs are not known.

The precise role of the α_1-adrenoceptor-mediated signal in embryonic cortical NPCs remains obscure, because the effects observed in the mixed-cell and organ culture experiments possibly reflect the secondary and tertiary effects mediated by multiple cellular interactions (glial cell-progenitor, neuronal cell-progenitor and neuronal cell-glial cell-progenitor interactions). As such, the aim of this study is to know the primary biological effect of α_1-adrenoceptor activation in the NPCs. We addressed the biological effects of α_1-adrenoceptor-selective agonists on highly purified embryonic NPCs. Our data indicate that these agonists inhibit death of NPCs cultured under various stress conditions but do not affect proliferation, differentiation or caspase-3/7-activity.

2. Materials and methods

2.1. Animals

Pregnant C57BL/6J mice were purchased from CLEA Japan (Tokyo, Japan). Animal care and handling were in accordance with institutional regulations for animal care and public law, and were approved by the Animal Investigation Committee of the National Institute of Neuroscience, Japan.

2.2. Antibodies and reagents

Monoclonal and polyclonal antibodies used in this study were as follows: monoclonal anti-nestin (Becton Dickinson, Lexington, KY), monoclonal anti-tuj1 (Covance, Berkeley, CA), polyclonal anti-glial fibrillary acidic protein (Dako, Carpinteria, CA), monoclonal anti-galactocerebroside (Chemicon International, Temecula, CA). The secondary antibodies conjugated to Alexa Fluor dye were purchased from Molecular Probes (Eugene, OR). α_1-adrenoceptor agonists used in this study were (*R*)-3-[1-hydroxy-2-(methylamino) ethyl] phenol (phenylephrine; Sigma, St. Louis, MO) and 2-[(2-cyclopropyl-phenoxy) methyl]-4, 5-dihydro-1H-imidazole (cirazoline; Tocris, Ellisville, MO). Each agonist was dissolved in Neurobasal™ medium (Invitrogen, Carlsbad, CA). Staurosporine and tunicamycin (Sigma) were dissolved in dimethyl sulfoxide (DMSO). Each solution was added to the medium, and the final concentration of DMSO in the medium was adjusted to at most 0.1% (v/v). Medium containing the same amount of organic solvent was used as a negative control.

2.3. Cortical NPCs culture

Cortical NPCs were cultured as previously described (Fukazawa et al., 2006). Briefly, embryos were removed from pregnant C57BL/6J mice and were staged according to morphological criteria to confirm gestational age. Developing mouse brain and cerebral cortex containing the ventricular and subventricular zones were dissected from embryonic day 14 (E14) embryos. Cells were mechanically dissociated by trituration and plated at 3.0×10^6 cells per 10-cm dish (BD) precoated with 15 μg/ml poly-L-ornithine (Sigma) and 1 μg/ml fibronectin (Nitta Gelatin, Osaka, Japan). Cells were expanded for 4 days in serum-free Neurobasal medium supplemented with 0.5 mM L-glutamine (Invitrogen), 100 U/ml penicillin, 100 μg/ml streptomycin (Invitrogen) and B27 (biotin, L-carnitine, corticosterone, ethanolamine, D(+)-galactose, glutathione (reduced), linoleic acid, linolenic acid, progesterone, putrescine, retinyl acetate, selenium, T3 (triodo-l-thyronine), DL-α-tocopherol (vitamin E), DL-α-tocopherol acetate, bovine serum albumin, catalase, insulin, superoxide dismutase, transferrin, vitamin A (Brewer et al., 1993); Invitrogen). N2 supplement (100 mg/l apo-transferrin, 5 mg/l insulin, 16 mg/l putrescine, 6.3 μg/l progesterone, 5 μg/l selenite; Sigma) were used for stress experiments instead of the B27 supplement. This medium was supplemented with 10 ng/ml basic fibroblast growth factor (bFGF; PeproTech, Rocky Hill, NJ) except when mentioned otherwise. Cultures were maintained at 37 °C in an atmosphere of 95% air and 5% CO_2. For secondary cultures, bFGF-expanded cortical NPCs were washed in warm Hanks' balanced salt solution, detached with mechanically pipetting, and resuspended in Neurobasal medium. Cells were then re-seeded on 24-well plates (Nunc; 1.8×10^5 cells/well), or 48-well plates (Nunc; 1.5×10^5 cells/well) precoated with poly-L-ornithine and fibronectin.

2.4. Real-time quantitative reverse-transcription (RT)-PCR

Real-time quantitative RT-PCR with the SYBR Green-based detection method was performed as previously described (Aoki et al., 2002). Total RNA was isolated from cultured cortical NPCs and E14 mouse cerebral cortex. These RNAs (1 μg) were treated with DNase I and converted to cDNA with Superscript II reverse transcriptase (Invitrogen) and random hexamer primers according to the manufacturer's instructions. The efficiency of reverse transcription and the quality of cDNA was compared with the efficiency of PCR amplification of the hypoxanthine guanine phosphoribosyl transferase (hprt) gene (GenBank accession ID. NM_013556; forward primer, 5′-TCTTTGCTGACCTGCTGGATT-3′; reverse primer, 5′-TATGTCCCCCGTTGACTGATC-

3′). Primers were designed for the α_{1A} (NM_013461), α_{1B} (NM_007416) and α_{1D} (NM_013460) adrenoceptor genes using Primer Express software (Perkin-Elmer, Torrance, CA). The forward and reverse primer sequences were as follows: 5′-TTTCAAGCCACCGGAAACA-3′ and 5′-ACTGGATTCGCAGCACATTCT-3′ (α_{1A}); 5′-AACCCTTCTACGCCCTCTTTTC-3′ and 5′-CCAGATTCTTGGTGGTCCTCTT-3′ (α_{1B}); and 5′-TCGCTCAAGTATCCAGCCATT-3′ and 5′-AACCTAGTAGCGGTCCCACAGA-3′ (α_{1D}). SYBR Green-based real-time RT-PCR was performed in 12.5-μl reactions (ABI PRISM 7700 Sequence Detection System, Perkin-Elmer). PCR products were analyzed with agarose gel electrophoresis. We checked each primer individually to ensure that the primer was selective for the target (data not shown). We also ensured that no band was observed in gel electrophoresis of PCRs that included distilled water or total RNA preparation without reverse transcriptase as template. The quantitative RT-PCR method (User Bulletin #2, Applied Biosystems, Foster City, CA) was modified to establish an expression level index for mRNA (Aoki et al., 2002), and the SYBR Green signal for the hprt amplicon was used as a reference. Amplification efficiency was determined and confirmed in a control PCR experiment using serial cDNA dilutions as templates. The real-time RT-PCR products were analyzed using the Applied Biosystems sequence detection system software 1.7.

2.5. LDH and ATP assay

The number of non-viable cortical NPCs was quantitatively assayed by measuring the activity of the cytosolic enzyme lactate dehydrogenase (LDH) released into the culture medium after membrane rupture. LDH activity was measured using the cytotoxicity assay CytoTox-ONE™ Homogeneous Membrane Integrity Assay (Promega, Madison, WI). To quantify the number of viable cells in cultured cortical NPCs, the amount of cellular ATP was measured using the CellTiter-Glo™ Luminescent Cell Viability Assay (Promega). These assays were performed in accordance with the manufacturer's protocol and on secondary cultured cortical NPCs as described above. Four hundred μl (1.5×10^5 cells/well) of cell suspension was added to each well of a 48-well plate (Nunc) precoated with poly-L-ornithine and fibronectin. After 24 h, cells were treated without or with 10 μM phenylephrine or cirazoline with different concentrations of bFGF or under different stress conditions as described in the figure legends. Cultures were then returned to the 37 °C incubator for 24 h, and assessment of LDH release in the media and amount of ATP was conducted with a Wallac 1420 multilabel counter (Perkin-Elmer, Finland).

2.6. Immunocytochemistry

Cells were stained as we have previously described with minor modifications (Sakurai et al., 2006). Briefly, all incubations and washes were performed at room temperature. Cells were fixed with 3.8% formaldehyde in phosphate-buffered saline (PBS) for 10 min and permeabilized with 0.02% (w/v) Triton X-100 in PBS for 5 min. Fixed cells were blocked with 3.3% goat serum in PBS for 30 min. Cells were incubated for 30 min with anti-nestin (neural progenitor marker; 1:500), anti-tuj1 (early neuronal cell marker; 1:500)(Sakurai et al., 2006), anti-glial fibrillary acidic protein (astrocyte marker; 1:1000) or anti-galactocerebroside (immature oligodendrocyte marker; 1:200)(Fukazawa et al., 2006). These cells were incubated with diluted secondary antibody (1:200) conjugated to Alexa Fluor for 30 min. All primary and secondary antibodies were diluted in 1% goat serum in PBS before use. The fluorescence microscopy images were obtained with an IX70 microscope (Olympus).

2.7. Quantification of enzymatic activities of caspases

Caspase-3 and caspase-7 protease activities were determined using the Caspase-Glo™ 3/7 Assay kit (Promega). All assays were performed on secondary cultured cortical NPCs as described above. Four hundred μl (1.5×10^5 cells/well) of cell suspension was added to each well of a 48-well plate (Nunc) precoated with poly-L-ornithine and fibronectin. After 24 h, cells were treated with or without 10 μM phenylephrine in medium lacking the N2 supplement as described in the figure legends. Cultures were then returned to the 37 °C incubator for 24 h, and caspase-3 and -7 activities were assessed with a Wallac 1420 multilabel counter.

2.8. Measurement of cell death using propidium iodide

All assays were performed on secondary cultured cortical NPCs as described above. Four hundred μl (1.5×10^5 cells/well) of cell suspension was added to each well of a 48-well plate (Nunc) precoated with poly-L-ornithine and fibronectin. After 24 h, cells were treated with or without 10 μM phenylephrine in medium lacking the N2 supplement. Cultures were then returned to the 37 °C incubator and maintained for 24 h, then stained with 1 μg/ml propidium iodide. Only dead cells with permeable plasma membranes were stained with propidium iodide. Positive controls were stained with propidium iodide after fixing with 3.8% formaldehyde in PBS for 10 min and permeabilized with 0.02% Triton X-100 in PBS. Dead cells and positive controls stained with propidium iodide were counted by fluorometry (Wallac 1420 multilabel counter).

2.9. Statistical analysis

Results are expressed as the mean±standard error of the mean (S.E.M.). Either the Student's *t*-test or Dunnett's multiple range test was used to evaluate the data using Prism software version 4.03 (GraphPad, San Diego, CA). Values of $P<0.01$ and $P<0.05$ were considered statistically significant depending on the specific experiment.

3. Results

3.1. Embryonic cortical NPCs express α_1-adrenoeceptor genes

We analyzed gene expression levels of the three α_1-adrenoceptors, and all were expressed both in the E14 embryonic